Journal of Materials Chemistry B

ROYAL SOCIETY OF CHEMISTRY

PAPER

View Article Online
View Journal | View Issue

Cite this: J. Mater. Chem. B, 2025, 13, 11790

Soft nanoparticles incorporating a benzo[c]xanthene fluorophore: facile synthesis and ratiometric pH sensing

Laura McKay,[a] Natali Joma,[b] Dusica Maysinger *[b] and Ashok Kakkar *[a]

Polymeric nanoparticles offer considerable potential in resolving key issues related to the delivery of small lipophilic pharmaceutics. However, significant challenges remain with respect to the development and application of multifunctional, easily accessible fluorescent tools for tracing the cellular uptake and trafficking of soft nanoparticles. We have evaluated a platform for this purpose utilizing the pH-responsive molecular sensor seminaphthofluorescein-C (benzo[c]xanthene 'SNAFL-C'); its chemical conjugation to an asymmetric miktoarm star polymer (AB_2) at its hydrophobic arm terminus; and traceable polymeric nanoparticles through self-assembly of SNAFL-AB_2 or physical encapsulation of the fluorophore. The characteristic high Stokes shift and ratiometric emission behaviour of SNAFL-C were retained in its polymer conjugate as well as in the self-assembled structures. Assemblies of the miktoarm fluorophore conjugate exhibited moderately reduced brightness as a result of aggregation induced quenching, an effect not observed for the physically encapsulated species. Fluorescence quenching experiments probing the partitioning of SNAFL-C in the core shell structures revealed localization of the primary fluorescent species in equilibrium based on their physiochemical properties, providing rationalization of differing aggregation behaviour observed for physically encapsulated and covalently linked formulations. Live cell fluorescence imaging in human glioblastoma cells integrating both SNAFL-C and its nanoformulations demonstrated the utility of the fluorophore in biological imaging applications and highlighted the necessity of detailed and stepwise spectral and photophysical evaluations. Collectively, these systems offer new avenues to explore fluorescence imaging using polymeric nanocarriers, leading to insights of broad importance to drug delivery and theragnostics.

Received 3rd June 2025,
Accepted 18th August 2025

DOI: 10.1039/d5tb01322d

rsc.li/materials-b

1. Introduction

Nanocarriers based on amphiphilic polymers continue to play a crucial role in improving the pharmacokinetics and efficacy of small molecule therapeutics. Linear block copolymers have in particular been widely investigated for the preparation of stable nanoformulations to transport and control the release of lipophilic active pharmaceutical agents.[1–7] More recently, the architecture and composition of the polymeric precursors to soft nanoparticles have been demonstrated to play a key role in tailoring their properties.[8] Miktoarm (mikto, Greek, meaning different) star polymers are branched structures possessing three or more polymeric arms radiating from a central core. This unique architecture has offered promise in drug delivery due to its exceptional synthetic tuneability in addition to the ability to form nanoparticles with low hydrodynamic sizes, dense hydrophilic coronas, low critical aggregation concentrations, and high loading efficiencies coupled with sustained cargo release.[9–11] To enhance our ability to deliver therapeutics effectively, and thus facilitate clinical translation, there is still an unmet need in understanding the intracellular fate of nanocarriers and their polymeric precursors.[12–15] The tracing of nanoparticles without inherent fluorescence, the primary method for non-invasive imaging with a high degree of spatio-temporal resolution, can be accomplished by the integration of fluorophores through covalent linkage to the polymeric precursor or direct physical encapsulation into their nanoparticles. The choice of strategy is highly dependent on the intended application of the system and synthetic considerations.[16–18] Significantly, the spectral and photophysical characteristics of formulations with covalently or physically incorporated species may diverge significantly from that of the free fluorophore as well as from each other. This essential and often overlooked aspect has important implications in optical imaging applications. An understanding of these two venues, tailored to

[a] Department of Chemistry, McGill University, 801 Sherbrooke St. West, Montreal, Quebec H3A 0B8, Canada. E-mail: ashok.kakkar@mcgill.ca
[b] Department of Pharmacology and Therapeutics, McGill University, 3655 Promenade Sir-William-Osler, Montreal, Quebec H3G 1Y6, Canada

specific polymer/fluorophore combinations, is central to addressing a wide variety of imaging needs including in the area of nanoparticle internalization and localization. Further, the development of theragnostic nanocarriers with a high degree of functionality is a rapidly developing field seeking to combine effective treatments with imaging capability for both diagnosis and monitoring. Such nanoparticles, often integrating small molecule organic fluorophores enable non-invasive optical imaging, play a key role in developing personalized precision medicine.[19–21]

The vast majority of work in the area of fabricating emissive soft nanoparticles employs commercially available fluorophores, primarily simple fluorescein and rhodamine derivatives. Fluorescein and its close relatives (BCEF, FITC) are ubiquitous in biomedical applications, including investigations of nanoparticle localization, for their exceptional brightness, low toxicity, and sensitivity to pH.[22–25] Although such compounds are highly accessible due to their commercial availability at low cost, specific spectral and photophysical properties of these dyes leave much to be desired. The notoriously low Stokes shifts of common xanthenes (<30 nm) are a significant limiting factor, as poor separation of excitation and emission bands is associated with low signal to noise ratios and self-quenching of fluorescence.[26–28] However, the most notable challenge associated with fluorescein and a bulk of other small molecule fluorophores is emission well under 550 nm, a range in which biological autofluorescence is significant. Imaging in the red region of the visible spectrum is highly sought after and has prompted extensive molecular engineering efforts to produce fluorophores emitting in the red to near IR.[29–32] Low energy excitation and emission is particularly favourable for deep tissue penetration, minimal interference from autofluorescence, and a reduced risk of phototoxicity to biological systems.[33,34]

Extension of the xanthene π system through benzannulation has been extremely successful as a strategy to red-shift the emission of fluorescein and related compounds.[35–37] The first systematic synthesis and investigation of a large set of these fluorophores is attributed to molecular probes (Invitrogen) in 1990.[38] This work brought forth two classes of asymmetric benzoxanthenes, termed seminaphthofluoresceins (SNAFLs, classified as fluoresceins) and seminaphthorhodafluors (SNARFs, categorised as rhodols). The shared features of these fluorophores included distinct absorbance and emission from the neutral and anionic species in the prototropic equilibrium (enabling ratiometric pH sensing, Scheme 1),

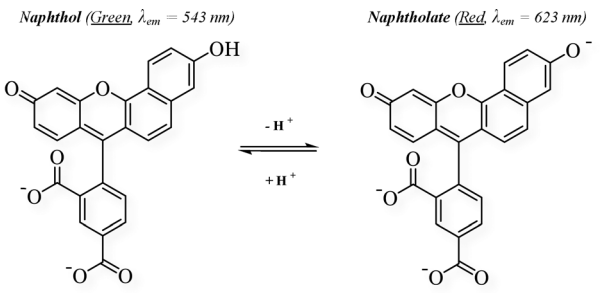

Scheme 1 Equilibrium of naphthol and naphtholate species determining the ratiometric emission behaviour of SNAFL-C.

exceptional Stokes shifts, and fluorescence stretching into the deep red. Intriguingly, the primary rhodol analogue seminaphthorhodafluor-C (SNARF-C, indicating benzannulation in the favourable 'C' position) has been extensively employed and is commercially available despite several limiting concerns. In direct comparison to SNAFL-C, the standout fluorophore from the original work by molecular probes, the quantum yield of the neutral state of SNARF-C is diminished approximately an order of magnitude, representing a significant detrimental decrease in brightness.[38] Additionally, discrepancies in pH quantification with SNARF-C have been identified and proposed to be a result of either reaction of the dimethylamino moiety with intracellular proteins or potential impurities in the commercially available material.[39,40] The initial commercialization and resulting continued prevalence of SNARF-C, despite the promising characteristics of SNAFL-C, appears closely tied to the push by molecular probes towards the marketing of rhodol type dyes in the 1990s.[41,42] This is an effect further compounded by the contemporary lack of simple, complete, and easily accessible information on the synthesis of SNAFL-C (and its analogue carboxy-SNAFL-C, hereafter termed simply SNAFL-C), culminating in the underutilization of this unique fluorophore.

In this study we sought to confer the exceptional features of SNAFL-C to polymeric soft nanoparticles while increasing ease to access of the fluorophore *via* practical synthetic information and updated detailed characterization. We have addressed outstanding deficiencies in the synthetic accessibility of SNAFL-C and present here a methodology with an improved isomer separation process. An analysis of costs for the commercial purchase of analogues (*e.g.* SNARF-C) and the presented synthesis highlights SNAFL-C as a model for the benefits of in-house preparation when paired with optimized, comprehensive procedures (see SI).

To expand our understanding of the internalization of polymeric nanoparticles upon entry into the biological medium, we have developed a simple and versatile strategy which includes (i) the facile, economic synthesis of high purity single isomer SNAFL-C; (ii) its covalent linkage to an AB_2 (A = polycaprolactone; B = polyethylene glycol) miktoarm polymer at its hydrophobic arm; and (iii) preparation of SNAFL-C containing nanoparticles by either physical incorporation into AB_2 miktoarm-polymer based assemblies, or by direct aqueous self-assembly of the SNAFL-AB_2 polymer conjugate (Scheme 2). The fluorophore exhibited a well-defined ratiometric response to pH, a result of the established equilibrium between the neutral naphthol and anionic naphtholate fluorescent species. A thorough spectral and photophysical evaluation of SNAFL-C enabled direct comparison of the properties of the fluorophore itself with the polymer conjugate unimer and nanoformulations. Covalent linkage of the fluorophore to the polymeric system was achieved through a simple esterification procedure in which chromatographic purification was not necessary to attain high purity. The optimized synthesis relied on the inherent reactivity of carboxy-SNAFL-C and polycaprolactone while exploiting solubility differences for purification. The resulting fluorescent conjugate (characterized with inhibition of self-assembly to isolate features of the unimer) was seen

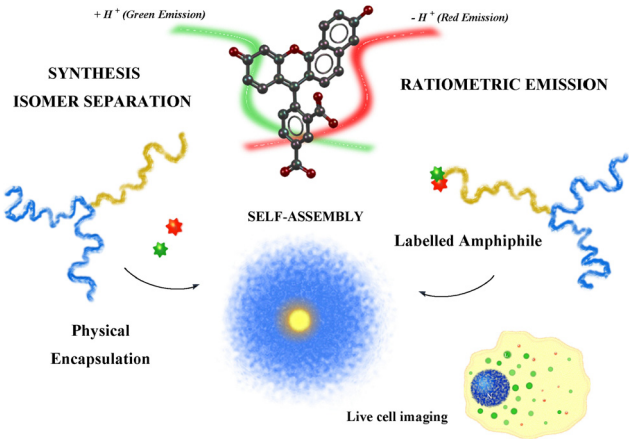

Scheme 2 Schematic representation of the scope of this work, highlighting major themes of (i) synthesis of single isomer SNAFL-C, a π extended fluorescein analogue exhibiting dual emission for ratiometric pH quantification (ii) preparation of fluorescent nanoformulations incorporating SNAFL-C *via* physical encapsulation and chemical conjugation alongside detailed spectral and photophysical analysis; and (iii) preliminary biological evaluation utilizing live cell fluorescence imaging.

to largely retain the original spectral and photophysical properties of SNAFL-C in the same medium. The unique solvent system employed to assess the optical properties of the conjugate unimer additionally provided an important pathway to evaluate the basic solvatochromism of SNAFL-C. Upon aqueous self-assembly, the conjugate (SNAFL-AB_2) formed micelles incorporating a high concentration of the fluorescent end group. These assemblies were seen to exhibit moderately diminished brightness resulting broadly from aggregation caused quenching effects. Conversely, physical encapsulation of SNAFL-C nanoparticles yielded a formulation with double the mass of fluorophore in relation to nanoparticles of the conjugate and no evidence of aggregation caused quenching effects.

An analysis of fluorophore microenvironments in both systems (assembled conjugate $\boldsymbol{\mu_2}$ and physically encapsulated SNAFL-C) using a dynamic quenching-based protocol offered a unique look into the differing localization of multiple species in the prototropic equilibrium. Further, these insights provided justification for the diverging aggregation effects in nanoformulations prepared by differing methods. Coupled with spectral data, quenching experiments carried out at neutral pH indicated that the neutral and anionic fluorescent species distributed independently in the core shell structure with: (i) the anionic naphtholate preferring to localize in the corona of both formulations; and (ii) the neutral naphthol at the core/shell boundary region when physically encapsulated, and deeper in the core when bound to the hydrophobic arm of the amphiphile. These results represent the first study involving simultaneous observation of multiple prototropic forms of a fluorophore within a nanostructure and offer a fresh perspective on the delicate balance between loading and brightness. Differences in the primary pK_a, representing the equilibrium between naphthol and naphtholate species, were quantified and linked to fluorophore localization. In addition to steady state measurements, this equilibrium was also explored *via* fluorescence lifetimes. A ring closure equilibrium, yielding a weakly fluorescent lactone in acidic conditions, was examined for the first time with respect to benzo[*c*]xanthenes in polymeric micelles. An understanding of SNAFL-C behaviour in acidic media was seen to be crucial to interpreting imaging results.

To establish translation to the more complex biological environment, ratiometric emission behaviour and response to intracellular pH variation were evaluated on glioblastoma cells using (i) free SNAFL-C and its masked diacetate analog; as well as (ii) chemically conjugated and physically encapsulated nanoparticle formulations. Through key differences in fluorescence emission and response to pH coupled with co-localization studies, insights into intracellular distribution were obtained.

2. Experimental

2.1 Materials and instrumentation

Purified water was obtained from a Millipore Milli-Q® (MQ) system. Monomer ε-caprolactone (Tokyo Chemical Industry, ≥99.0%) was dried over calcium hydride for 48 h and distilled under reduced pressure. Tin(II) 2-ethylhexanoate (Sigma Aldrich) was dried over activated molecular sieves for 48 h and distilled before use. All other reagents and solvents were purchased from Sigma Aldrich or Oakwood Products and used as received. Anhydrous solvents were passed through activated alumina in an MBraun solvent purification system. Dialysis membranes (Spectrum™ Spectra/Por™, MWCO: 3.5 kDa) were purchased from Fisher Scientific. Solvents for NMR analysis were purchased from Cambridge Isotope Laboratories and used as received. Column chromatography was performed using silica gel 60 (230–400 mesh) from Silicycle Inc. ^{1}H and ^{13}C NMR characterizations were performed on a Bruker AVIIIHD 500 MHz NMR spectrometer. Dulbecco's modified Eagle medium (DMEM, 11965084), Hoechst 33342 and penicillin–streptomycin were purchased from Thermo Fisher Scientific. Fetal bovine serum was supplied by Wisent Inc. A Bruker MALDI Autoflex III-TOF was used for mass spectra determination. Gel permeation chromatography (GPC) was performed on a Waters Breeze GPC system with HPLC grade THF as the mobile phase. Particle size measurements utilized a Brookhaven90Plus Particle Size Analyser equipped with a 40 mW red diode laser. A Thermo Scientific Talos F200X with a Ceta 16 M 4k × 4k CMOS camera was employed for transmission electron microscopy (TEM).

UV-Vis absorption spectra were recorded on a Agilent Cary 50 spectrophotometer and fluorescence measurements were carried out on a Agilent Cary Eclipse spectrophotometer with slit widths fixed at 5 nm. Extinction coefficients were determined by calibration according to the Beer–Lambert law. Fluorescence lifetimes were obtained with an Edinburg instruments Mini-tau unit by time correlated single photon counting (TCSPC). Stern Volmer quenching constants and equilibrium constants were reported with error at the 95% confidence level. Chemical shifts (δ) were reported in parts per million (ppm)

relative to tetramethylsilane using the residual solvent peak as a reference. Relative quantum yields were reported with reference to commercial rhodamine 101 by the following equation in which 's' and 'r' denote sample and reference, respectively. Concentrations were adjusted to keep absorbance at (and above) the excitation wavelength below 0.1 AU with differences in refractive index accounted for. Values are reported as determined quantum yield ± propagated error.

$$\Phi_s = \Phi_r \left(\frac{m_s}{m_r}\right)\left(\frac{n_s}{n_r}\right)^2$$

2.2 Methods

2.2.1 Preparation of soft nanoparticles. Aqueous self-assembly of blank and loaded micelles was carried out by the co-solvent evaporation method.[43] Solutions containing 5.0 mg of miktoarm polymer $\boldsymbol{\mu_1}$ or $\boldsymbol{\mu_2}$ and 1.0 mg of cargo (where applicable) were prepared in 2.0 mL of HPLC grade acetone and added at a fixed rate of 1 drop per 5 seconds to a 2.0 mL solution of MQ water being stirred at 400 rpm. The solutions were protected from light and stirred for 18 h under ambient fume hood pressure to completely remove the organic solvent and trigger micelle formation. Complete removal of the organic phase was confirmed by mass tracking. The aqueous solutions were passed twice through 0.22 μm polyvinylidene fluoride (PVDF) syringe filters. Aliquots were taken for DLS measurements to determine hydrodynamic diameters and polydispersity index of the resulting micelles. For determination of micelle cargo (SNAFL-C) content by UV-vis, aliquots were removed and diluted by a factor of 48 with ethanolic potassium hydroxide. The utilized standard curve for SNAFL absorption is provided in the SI (Fig. S.39). Encapsulation efficiency and loading capacity of the nanocarriers were calculated by mass according to the following equations.

$$\text{Encapsulation efficiency (EE)}\% = 100 \times \left(\frac{\text{Loaded cargo}}{\text{Total added cargo}}\right)$$

$$\text{Loading capacity (LC)}\% = 100 \times \left(\frac{\text{Loaded cargo}}{\text{Loaded cargo} + \text{polymer}}\right)$$

In a representative TEM experiment 15 μL of the micellar solution (previously diluted 10× with MQ water) was dropped on a carbon-coated copper grid, with excess solution removed by a Whatman filter paper after five minutes. Subsequently 15 μL of 2% uranyl acetate was applied to the grid for a period of one minute. The stained grid was allowed to dry for a minimum of thirty minutes before imaging. Critical micelle/aggregation concentration (CMC/CAC) was determined by the pyrene 1 : 3 method in which a range of polymer concentrations were prepared in 6 μM solutions of pyrene in THF.[44] The organic solutions were added at a rate of 1 drop/5 s into 1 mL solutions of MQ and allowed to stir protected from light until the evaporation of THF was complete as indicated by mass. Fluorescence excitation spectra were recorded with the emission wavelength fixed at 390 nm.

2.2.2 Cell culture. U251N human glioblastoma cells (derived from a 75-year-old male patient with brain astrocytoma) were originally obtained from the American type culture collection. Unless otherwise specified, cells were maintained in Dulbecco's modified Eagle medium, supplemented with 5% (v/v) fetal bovine serum, and 1% (v/v) penicillin–streptomycin at 37 °C with 5% CO_2 and 95% relative humidity.

2.2.3 Cell counting and treatment. Confluent monolayer cell cultures of 70–80% were detached using 0.05% trypsin–EDTA, seeded at 7000 cells per coverslip, and cultured for 24 h. When appropriate cells were treated with chloroquine (CQ) for 24 hours. SNAFL-C (1.5 μM), SNAFL diacetate **4** (1.5 μM), conjugated SNAFL-C $\boldsymbol{\mu_2}$ nanoparticles (1.5 μM), or encapsulated SNAFL-C in nanoparticles of $\boldsymbol{\mu_1}$ (1.5 μM) were added 30 minutes prior to imaging.

2.2.4 Cell viability. Confluent monolayer cell cultures of 70–80% were detached using 0.05% trypsin–EDTA, seeded in 96-well cell culture plates at 7000 cells per well, and cultured for 24 h. Cells were treated with increasing concentrations of SNAFL for 24 h. Nuclei were labeled with Hoechst 33342 (10 μM, Thermo Fisher Scientific) for 30 min. Cells were imaged using a fluorescence microscope (Leica DMI4000B) with the UV filter at 10× magnification.

2.2.5 Fluorescence imaging. Nuclei were labeled with 10 μM Hoechst 33342 for 30 min. Coverslips were washed twice with PBS. Fluorescence signals were detected using fluorescent live imaging with GFP and CY5 filters. Cells were imaged using a fluorescence microscope (Leica DMI4000B) with the UV filter set at 60× magnification.

2.2.6 Preparation of 5(6)-carboxyfluorescein (1)[45]. A one neck 100 mL round bottom flask was charged with 9.23 g of resorcinol (84.2 mmol) and 8.06 g of 1,3-dioxo-2-benzofuran-5-carboxylic acid (41.9 mmol) before dissolution in 60 mL of methane sulfonic acid. The mixture was brought to 80 °C for a period of 18 h. After cooling to room temperature, the reaction mixture was poured slowly into 500 mL of cooled deionized water with fast stirring. The resulting orange precipitate was allowed to settle before collection on a medium grain frit where it remained for 24 h under house vacuum. The solid material was transferred to a conical flask with the addition of 150 mL of absolute ethanol. The mixture was allowed to heat to 60 °C with stirring until homogenous. After removal from heat, 400 mL of deionized water was added over a period of 20 minutes with vigorous stirring of the solution. The solid was allowed to settle at room temperature before collection on a frit. After 48 h under house vacuum the material was dried *in vacuo* to yield 15.35 g (40.8 mmol, 97%) of the title compound as a fine orange powder. Full removal of trace water without the use of high temperatures was achieved by dissolution of **1** into ethyl acetate, washing with small portions of saturated brine solution, drying of the organic phase by magnesium sulfate and removal of solvent, followed by a period of 1 h under high vacuum.

2.2.7 Preparation of 4-(2,4-dihydroxybenzoyl)isophthalic acid (2). To a one neck 250 mL round bottom flask equipped with a condenser was added 80 mL of deionized water.

In portions 80.0 g of sodium hydroxide pellets (50% by mass) were added to solution. After a cooling period of 45 minutes 10.22 g of **1** (27.0 mmol) was added to the flask. The deep purple solution was heated to 95 °C for a period of 24 h. The medium brown mixture was cooled to room temperature before slow addition to 300 mL of chilled deionized water in a 1 L beaker. The flask was placed in a secondary ice/brine bath and set to stir vigorously before initiating dropwise addition of 12 M HCl. The addition was continued over a period of 2 h and slowed as the solution reached acidity. At a pH of ~1 a beige solid precipitated rapidly, at which point the stirring rate was increased and addition was stopped. The solids were allowed to stir for 1 h and settle overnight at room temperature. The crude product was collected on a medium grain frit and dried for 24 h on house vacuum. After an additional 1 h under high vacuum the solid was taken up in 200 mL of diethyl ether and washed with 50 mL portions of water and brine. The ethereal solution was dried with magnesium sulphate and the solvent removed under reduced pressure to yield 6.86 g of 2-(2,4-dihydroxybenzoyl) terephthalic acid and 4-(2,4-dihydroxybenzoyl) isophthalic acid as a 1 : 1 isomer mixture (22.7 mmol, 84%). Crucially, foaming of the product under vacuum to a fine shiny powder takes place when the sample is sufficiently dry and suitable for recrystallization. Following the initial observation of foaming, an additional 30 minutes under reduced pressure yields an ideal, easily handled solid. Material which remains as a viscous liquid or amorphous solid may be repeatedly mixed with small volumes of ether and dried under vacuum until observation of foaming to the desired powder. Portions of the dried sample were then taken for isomer separation as required. In a representative experiment 1.80 g of the dried mixture was transferred to a 50 mL beaker and dissolved in 9 mL of HPLC grade methanol (suggested concentration: 2 g mL^{-1}). After confirmation of full and immediate dissolution of the solids, 18 mL of deionized water (1 : 2 ratio of methanol/water) was slowly added to the homogenous solution in increments with manual mixing. Partial or slow dissolution of the compound in methanol is indicative that the material is not suitably prepared for recrystallization and should be subjected to additional drying cycles. The flask was subsequently sealed and left undisturbed at room temperature for a period of 1 h as crystallization took place. The resulting solids were collected on a coarse frit and allowed to dry under house vacuum. The mother liquor was set aside for 48 h to allow precipitation of remaining material (reclaimed and subsequently dried for future recrystallization) or, alternatively, directly extracted with ether. The crystalline material was then taken up into 50 mL of ether and washed with 2 × 10 mL portions of brine. Drying with magnesium sulphate and removal of solvent yielded 0.75 g of a fine light yellow solid (^{1}H NMR: 90% 4-(2,4-dihydroxybenzoyl)isophthalic acid/10% 2-(2,4-dihydroxybenzoyl)terephthalic acid). The material underwent a secondary recrystallization *via* the same procedure (3 mL methanol: 6 mL water, crystallization time period of 15 minutes) to yield 0.45 g (50% of compound **2**) of the pure regioisomer as a fine light-yellow powder.

2.2.8 Preparation of 5-carboxy-seminaphthofluorescein (SNAFL-C, 3)[46]. A two neck 50 mL round bottom flask under nitrogen was charged with 0.72 g (2.4 mmol) of **2** and 0.42 g (2.6 mmol) of 1,6-naphthalene diol. Through a rubber septum 10 mL of methane sulfonic acid and 10 mL of trifluoroacetic acid were added and the reaction was allowed to proceed at room temperature, shielded from light, for 24 hours. The teal solution was then opened to air and poured into 250 mL of chilled deionized water with immediate precipitation of the crude product. The deep purple solid was collected on a fine grain frit, washed with 3 × 10 mL portions of water on the frit, and allowed to dry under house vacuum for 24 h. A solution of the crude product in 100 mL of 2 M NaOH was prepared in a 500 mL conical flask. Dropwise addition of 120 mL of 2 M HCl with vigorous stirring resulted in precipitation of a fine purple solid which was collected and dried thoroughly under vacuum. The collected material was dissolved in 50 mL of anhydrous ethanol and added dropwise to 200 mL of deionized water with vigorous stirring. The resulting precipitate was allowed to settle at room temperature before collection on a fine grain frit. After drying under low vacuum, the solid was subjected to 3 cycles of dissolution in acetone, removal of solvent, and exposure to high vacuum. The title compound, a shiny deep purple solid reflecting green, was obtained in 53% yield (0.54 g, 1.3 mmol).

2.2.9 Preparation of 5-carboxy-seminaphthofluorescin diacetate (4). Under nitrogen flow fluorophore **3** (0.39 g, 0.91 mmol) was dissolved in 15.0 mL of fresh acetic anhydride. Pyridine (50 μL) was added *via* syringe through rubber septum and the mixture was brought to 110 °C for a period of 1 h. After cooling bulk acetic anhydride was removed by rotary evaporation. An azeotrope (ethyl acetate) was utilized to eliminate the remaining solvent. The brown solid was taken up in 25 mL of ethyl acetate and washed with 15 mL each of 0.5 M HCl and brine. The organic layer was dried over magnesium sulphate and the solvent was removed under reduced pressure. The target compound, an off-white powder, was isolated by recrystallization from anhydrous ethanol (0.23 g, 49%).

2.2.10 Synthesis of (3,5-bis(prop-2-yn-1-yloxy)phenyl)methanol (5). A two neck round bottom flask was charged with 3,5-dihydroxybenzyl alcohol (1.00 g, 7.14 mmol), potassium carbonate (1.30 g, 9.28 mmol), and 18-crown[6] under a nitrogen atmosphere. The reagents were dissolved in 30 mL acetone, treated with propargyl bromide (80% in toluene – 1.6 mL, 14.3 mmol) and brought to 60 °C. After 18 hours the solution was cooled and the solvent was removed under reduced pressure. The resulting oily solid was then dissolved in dichloromethane and extracted from water three times. The combined organic layers were dried over magnesium sulfate and the solvent was removed under reduced pressure. The crude residue was dry loaded onto a moderate length column and eluted with 2 : 1 hexanes/ethyl acetate to yield 1.15 g (75%) of **5** as a crystalline white solid.

2.2.11 Preparation of polycaprolactone (6). A dried three neck round bottom flask was charged with compound **5** (0.24 g, 1.1 mmol), distilled ε-caprolactone (2.50 mL, 22.6 mmol), and 40 mL dry toluene under a nitrogen atmosphere. The mixture was heated to 100 °C, at which time distilled and nitrogen

purged Sn(II) ethyl hexanoate (0.070 mL, 0.226 mmol) was added in one portion *via* syringe. The solution was allowed to reflux at 110 °C for 18 hours under nitrogen. After cooling to room temperature, the solvent was removed under reduced pressure. The resulting oil was dissolved in minimal dichloromethane and precipitated in ice cold methanol. The precipitated solid was collected by filtration and dried *in vacuo* to yield 2.70 g (93%) of **6** as a fine white powder.

2.2.12 Preparation of $mPEG_{2000}$–N_3 (7). In a two neck round bottom flask under a nitrogen atmosphere, commercial $mPEG_{2000}$–OH (4.42 g, 2.18 mmol) was dissolved in 40 mL dichloromethane. The solution was cooled to 0 °C in an ice bath and subsequently treated with 4-dimethylaminopyridine (0.07 g, 0.572 mmol), *p*-toluene sulfonyl chloride (0.53 g, 2.77 mmol), and triethylamine (2.0 mL, 14.3 mmol) in sequence. The mixture was allowed to warm to room temperature overnight at which time the solvent was removed under reduced pressure. The crude mixture was dissolved in 25 mL chloroform and washed with two 10 mL portions of 0.1 M HCl solution and 10 mL of brine. The organic layer was dried over magnesium sulfate and the solvent was removed under reduced pressure to yield 4.65 g (97%) of the mono-tosylated polymer $mPEG_{2000}$–OTs as a white solid. In a one neck round bottom flask 40 mL of anhydrous ethanol was added to $mPEG_{2000}$–OTs (1.52 g, 0.71 mmol) and sodium azide (0.15 g, 2.1 mmol). The solution was heated at 80 °C for 20 h at which time the solvent was carefully removed under reduced pressure. The crude oil was dissolved in 50 mL of chloroform and washed with 50 mL of distilled water. The aqueous layer was then extracted with three 50 mL portions of chloroform. The combined organic fractions were washed with a portion of brine and dried over magnesium sulfate before removal of the solvent under reduced pressure. The resulting oil was dissolved in minimum dichloromethane and precipitated in ice cold ether. Collection by filtration and drying under vacuum yielded 1.12 g (78%) of the title polymer as a white solid.

2.2.13 Preparation of PEG_2–PCL (μ_1). $mPEG_{2000}$–N_3 **7** (0.32 g, 0.16 mmol) and **6** (0.18 g, 0.072 mmol) were added to a dried two neck round bottom flask under a nitrogen atmosphere and dissolved in dry dimethylformamide (7 mL). Separately, purified CuBr (0.016 g, 0.108 mmol) and *N*,*N*,*N*′,*N*″,*N*,″ pentamethyldiethylenetriamine (0.020 mL, 0.108 mmol) were added to a dry one neck flask under a nitrogen atmosphere with 1 mL of dry dimethylformamide. This mixture was added dropwise to the primary reaction flask and the resulting blue solution was stirred at 40 °C for 24 hours. After completion the solvent was removed under reduced pressure, utilizing a toluene azeotrope. The crude product was dissolved in dichloromethane and washed with a 1 M aqueous ethylenediaminetetraacetic acid (EDTA) solution which was then extracted three times. The combined organic fractions were combined and dried over magnesium sulfate. Removal of the solvent with reduced pressure yielded a light yellow oil which was subsequently dissolved in minimal tetrahydrofuran and placed in a 3.5 kD dialysis membrane. The product was dialyzed against 300 mL of an 85 : 15 tetrahydrofuran/water mixture for 48 hours. The solution remaining in the membrane was removed and dried under reduced pressure. The resulting residue was dissolved in minimal dichloromethane and precipitated with ice cold ether to yield 0.29 g (60%) of μ_1 as a fine white solid.

2.2.14 Preparation of polycaprolactone-SNAFL (8). In a dried two neck round bottom flask protected SNAFL **4** (0.29 g, 0.58 mmol), polycaprolactone **6** (0.78 g, 0.29 mmol) and 4-dimethylaminopyridine (0.018 g, 0.15 mmol) were dissolved in 3 mL of dry dichloromethane. The mixture was cooled in an ice bath for 30 minutes, at which time a 0.5 mL solution of *N*,*N*′-dicyclohexylcarbodiimide (0.070 g, 032 mmol) was added dropwise through a rubber septum. The reaction was allowed to equilibrate to room temperature overnight under nitrogen flow and protected from light. At 48 h the mixture was cooled in the freezer and subsequently passed through a syringe filter to remove the precipitated urea byproduct. The solution was diluted with a further 75 mL of dichloromethane and washed with 40 mL of 0.1 M HCl followed by the same volume of brine. After drying over magnesium sulfate and removal of solvent the solid was dissolved in minimal dichloromethane and precipitated with 200 mL of cold methanol. The resulting solids were collected on a medium frit and subjected to a second precipitation by the same solvent system. The title compound was obtained as a beige solid (0.51 g) in 55% yield.

2.2.15 Preparation of PEG_2–PCL–SNAFL (μ_2). $mPEG_{2000}$–N_3 **7** (0.56 g, 0.28 mmol) and polycaprolactone **8** (0.42 g, 0.13 mmol) were added to a dried two neck round bottom flask under a nitrogen atmosphere and dissolved in dry dimethylformamide (5 mL). Separately, purified CuBr (0.028 g, 0.20 mmol) and *N*,*N*,*N*′,*N*″,*N*″, pentamethyldiethylenetriamine (0.040 mL, 0.20 mmol) were added to a dry one neck flask under a nitrogen atmosphere with 1 mL of dry dimethylformamide. The mixture was added dropwise to the primary reaction flask and the resulting solution was stirred at 40 °C for 24 hours. A colour change from blue to a vibrant purple took place over a 20-minute period. After completion, the solvent was removed under reduced pressure (azeotrope with toluene). The crude product was dissolved in dichloromethane and washed with a 1 M EDTA solution which was then extracted an additional three times. The organic fractions were combined and dried over magnesium sulfate. Removal of solvent with reduced pressure yielded a magenta oil which was dissolved in minimal tetrahydrofuran and placed in a 3.5 kD dialysis membrane. The product was dialyzed against 300 mL of an 85 : 15 tetrahydrofuran/water mixture for 48 hours. The solution remaining in the membrane was removed and dried under reduced pressure. The residue was dissolved in minimal dichloromethane and precipitated with ice cold ether to yield 0.46 g (49%) of μ_2 as a pink solid.

3. Results and discussion

3.1 Fluorophore synthesis and polymer labelling

3.1.1 SNAFL-C. While symmetric fluoresceins are traditionally produced in a single step by a modified Freidel Crafts reaction, asymmetric seminaphthofluoresceins and rhodafluors

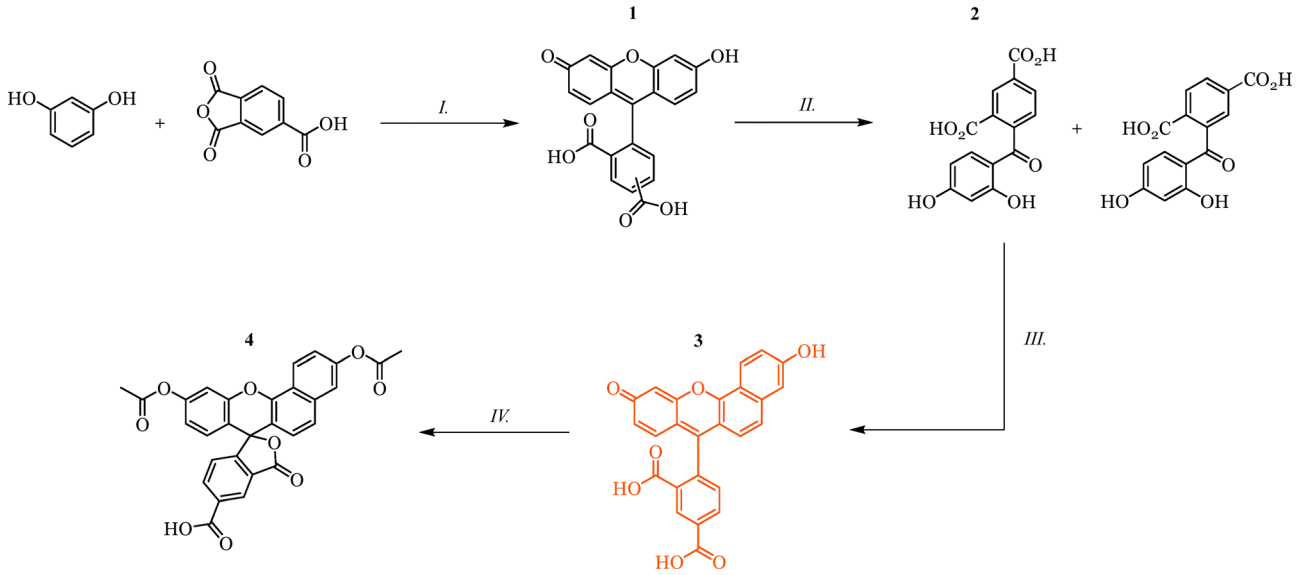

Scheme 3 Synthesis and protection of single isomer SNAFL-C (**3**). (I) $MeSO_3H$, 80 °C, 18 h. (II) 50% NaOH (aq.), 95 °C, 24 h. (III) 1,6-Naphthalene diol, $MeSO_3H$/TFA, RT, 24 h. (IV) Acetic anhydride, pyridine, 110 °C, 1 h.

are commonly accessed through fluorescein and its hydrolysis to a versatile benzophenone intermediate.[35,38,47] To establish a synthetic handle suitable for conjugation to the polymeric species, we chose to employ the carboxylic acid derivative of seminaphthofluorescein-C, as illustrated in Scheme 3. Installation of this moiety first involves replacement of the phthalic anhydride starting material in the synthesis of fluorescein with the trimellitic anhydride, yielding a 1 : 1 mixture of regioisomers termed 5,6-carboxyfluorescein.

Despite the addition of this functionality having little bearing on the optical properties of the fluorophore, behaviour begins to diverge following esterification based on the position of the carboxylic acid on the lower ring. The extensive investigation of carboxy-fluoresceins and related derivatives has provided important insights into the distinct behaviour of the common isomers (possessing secondary carboxylic acids in the 5 or 6 positions).[48] Significantly, esterification in the 6 position results in a substantial reduction of fluorescence quantum yields while the corresponding 5-ester experiences only a minor suppression of overall brightness.[49,50] This phenomenon has been attributed to a photoinduced electron transfer process (PeT) from the excited state xanthene HOMO to the benzene LUMO. While the labelling of both positions results in an energetic decrease of the LUMO associated with the benzene moiety, this effect is less pronounced for the 5′ isomer and the quenching associated with the photoinduced electron transfer is limited. For this reason, isolation of the 5 isomer is broadly desired for applications in which the carboxylic acid moiety undergoes esterification. While carboxy-fluorescein and its analogues are most commonly sold as isomeric mixtures, lack of commercial demand for single isomer fluoresceins and rhodafluors is likely a result of the staggering cost of these products rather than an indication of lack of utility (Table S.5). A limited number of literature procedures for isomer separation exist but these often remain largely inaccessible for those outside of a narrow range of expertise due to the necessity of complex purification methods, and/or sparse detail in published methodologies.[51–54]

We present here a detailed and simple methodology for the in-house synthesis of single isomer SNAFL-C, bringing together insights from several published procedures while providing additional practical methodological information and an improved approach to isomer separation. Carboxy-fluorescein was first synthesized by the well-established double Freidel Crafts reaction of resorcinol and trimellitic anhydride in methanesulfonic acid. After quenching of the reaction and a secondary precipitation of the crude product in ethanol/water, the material underwent extensive drying to yield an equal mixture of 5 and 6-carboxyfluorescein with no observable impurities. Hydrolysis of this material in a 50% solution of sodium hydroxide with subsequent acidification and precipitation steps yielded the benzophenone intermediate as a 1 : 1 isomer mixture. Isomer separation at this stage, an already vital intermediate in the synthesis of asymmetric xanthenes, was highly cost and time effective. Selective recrystallization of these benzophenones, reported by Hammershøj *et al.* in 2015, exploits differing crystallization kinetics of the isomers in methanol/water solutions.[55] However, the published procedure lacks repeatability and requires lengthy recrystallization times, noted as 2–3 repetitions of 1+ week each to achieve a 36% yield.

In this work we emphasize the necessity of additional dehydration steps and provide rules of thumb for the concentration (0.5 g mL^{-1} of methanol) and composition of the recrystallization mixtures (1 : 2 methanol/water). Extensive drying before separation, in which the suitably prepared compound is easily identified by foaming of the material to a fine powder under reduced pressure, functions not only to reduce crystallization time to under two hours but also aids

in improving repeatability of the procedure. In the final step, condensation of the purified benzophenone with 1,6-dihydroxynaphthalene in a 1 : 1 mixture of methanesulfonic acid and trifluoroacetic acid produces single isomer SNAFL-C (**3**). Precipitations during work up allow for isolation of the fluorophore in high purity without the need for chromatographic purification techniques. The ability to synthesize high purity single isomer SNAFL-C without column purification is significant in the context of accessibility, particularly when coupled with a simplified and time efficient isomer separation process. A complete analysis of the costs of in-house synthesis and estimated commercial pricing is provided in the SI (Tables S.3–S.5).

While charged functional groups are known to increase the retention of dyes in cells, these fluorophores are traditionally introduced as their neutral 'membrane permanent' esters. For this purpose, SNAFL-C was converted to non-fluorescent diacetate **4** *via* acetylation with acetic anhydride. Diacetates of this type are designed to undergo cellular internalization easily and subsequently be hydrolyzed by intracellular esterases to yield the charged (and thus well retained) compound with restored fluorescence.[56–58] The secondary carboxylic acid functional group of SNAFL-C, deprotonated at neutral pH, can be expected to further contribute to enhanced retention of the species in cells.[59]

3.1.2 Fluorophore labelled and unfunctionalized miktoarm polymers. The fabrication of well defined, low polydispersity miktoarm polymers is best achieved through a modular ligation approach involving a series of simple and high yielding reactions.[60,61] As depicted in Scheme 4 we synthesized the non-emissive AB_2 miktoarm polymer $\boldsymbol{\mu_1}$, comprised of one polycaprolactone (A = PCL) block and two polyethylene glycol (B = PEG) arms branching from a central core. Propargylation on the heterobifunctional core was followed by the ring opening polymerization of caprolactone. Azide terminated polyethylene glycol ($mPEG_{2000}$–N_3) was synthesized separately by tosylation and subsequent azidation from commercially available monomethoxy polyethylene glycol of a molecular weight of ~2000 g mol^{-1}. Copper(I) catalyzed alkyne–azide cycloaddition was then utilized to link the hydrophilic and hydrophobic components, generating the desired miktoarm polymer $\boldsymbol{\mu_1}$. In the context of linking the fluorophore to the polymeric system, the hydroxyl end group of polycaprolactone is well suited for direct esterification with the secondary carboxylic acid of **3**. However, SNAFL-C appeared to undergo intermolecular esterification in the presence of coupling agents, preventing formation of the desired product (Fig. S.32 and S.33). Substitution of SNAFL-C (**3**) with acetylated analogue **4** eliminated this pathway, allowing for clean labelling of the polymer. The increased solubility of the protected compound in a wide range of organic solvents additionally enabled the use of traditional Steglich esterification conditions.[62] Direct reaction of excess diacetate **4** with polycaprolactone **6** vastly simplified purification in comparison to reaction with an amphiphile such as $\boldsymbol{\mu_1}$. The labelled polycaprolactone was readily precipitated by a dichloromethane/methanol solvent system, while the excess fluorophore remained soluble and was thus readily removed. The high molecular weight of SNAFL-C assisted in characterization, as the difference in molecular weight between the unlabelled and dye functionalized polymer was observable by both GPC and MALDI-TOF analysis. The established Cu(I) CuAAc 'click' methodology was then employed to ligate the two hydrophilic arms. The acetate protecting groups on the fluorophore were rapidly cleaved in this step, removing the need for an additional reaction to generate fluorescent $\boldsymbol{\mu_2}$. The resulting miktoarm polymer was characterized using a combination of techniques including NMR and GPC (see SI).

3.2 Spectral and photophysical characterization of SNAFL-C and polymer conjugate

3.2.1 SNAFL-C. We first evaluated the unique spectral and photophysical characteristics of SNAFL-C, as presented in Table 1.

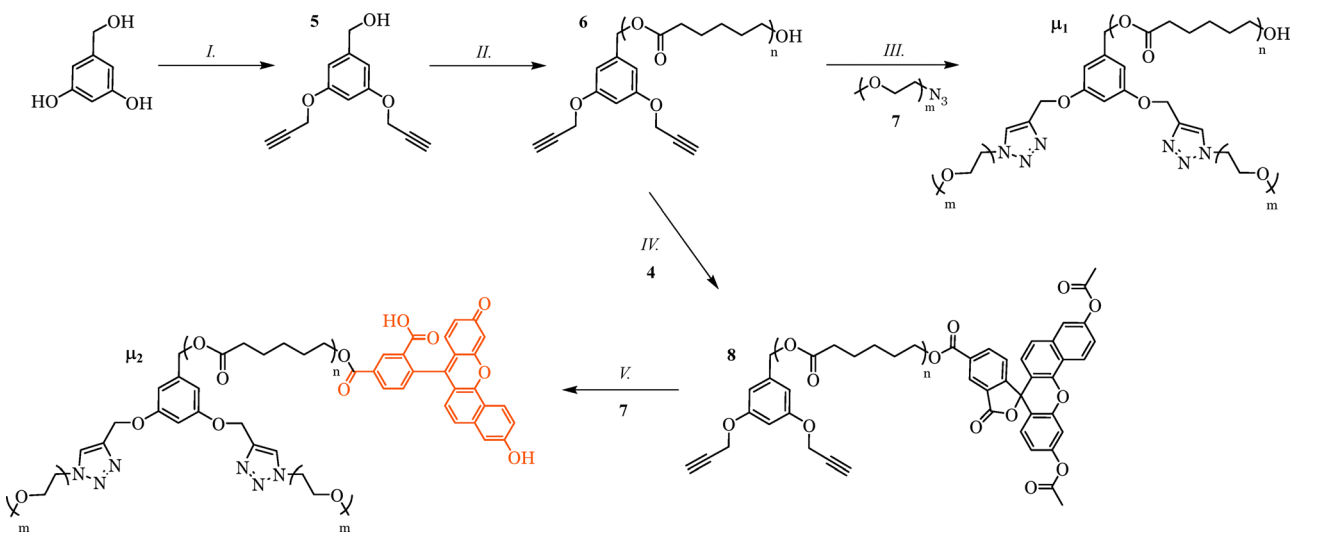

Scheme 4 Synthesis of miktoarm polymers $\boldsymbol{\mu_1}$ (unlabelled PEG_2–PCL) and $\boldsymbol{\mu_2}$ (fluorescent PEG_2–PCL–SNAFL). (I) Propargyl bromide, K_2CO_3, 18-crown[6], acetone, 60 °C, 18 h. (II) ε-Caprolactone, tin(II) ethyl hexanoate, toluene, 110 °C, 18 h. (III) $mPEG_{2000}$–N_3 (**7**), CuBr, *N*′*N*′-PMDETA, DMF, 40 °C, 24 h. (IV) SNAFL-diacetate (**4**), DCC/DMAP, DCM, 0 °C – RT, 48 h. (V) CuBr, *N*′*N*′-PMDETA, DMF, 40 °C, 24 h.

Table 1 Selected properties of SNAFL-C at representative acidic (naphthol, PBS buffer) and basic (naphtholate, carbonate/bicarbonate buffer) pH conditions

pH	λ_{abs}/nm	ε_{max}/M^{-1} cm^{-1}	λ_{em}/nm	Stokes/nm	pK_a	Φ_f	τ/ns
10	540	46 900	623	83	—	0.086 ± 0.008	1.21
6	511 485	26 400	543	58	7.81	0.35 ± 0.03	3.53

Consistent with the original work of Whitaker *et al.* the fluorophore showed well-defined responses in its absorption and emission spectra to changes in pH (Fig. 1).[38] The properties of the two fluorescent species responsible for the ratiometric emission behaviour of SNAFL-C, shown in Scheme 1, were readily isolated with appropriate solution pH. The neutral naphthol was dominant at pH 6, with two primary absorption bands at 485 and 511 nm. In alkaline conditions deprotonation occurred, yielding the anionic naphtholate absorbing at 540 nm. In direct comparison to fluorescein in the anionic state, the absorbance of SNAFL-C was red-shifted by an impressive 49 nm.[23] The associated pK_a was determined to be 7.81, a desirable near neutral value in the physiological range (Fig. S.64).

The emission bands of the two species were seen to be distinct and well resolved. Naphthol emission was centred at 543 nm with a shoulder at 600 nm, a feature attributed to the excited state proton donating character of the species. The naphtholate emission band was symmetric, with a maximum at 623 nm and intensity extending to 800 nm. The anion, with a Stokes shift of 83 nm, represents a striking 117 nm bathochromic shift in emission from the equivalent fluorescein species.[23] The simple, well-defined equilibrium is illustrated by the presence of a clear isosbestic point in the pH dependent absorbance spectra (Fig. S.42). It is this equilibrium which imparts the capability for ratiometric pH detection, as demonstrated in Fig. 2. While the bulk of pH responsive fluorophores rely on the simple modulation of emission intensity, SNAFL-C is established to function as ratiometric pH sensor. In the context of fluorescence, ratiometric sensors (broadly based on interplay between two well resolved absorbance or emission bands) fall into two primary categories, single compound or specifically fabricated materials incorporating two fluorophores. When utilized for pH measurement, these determinations are exceptionally accurate and not subject to environmental factors.[63–65] In contrast, measurements employing fluorescence intensity based methods (measuring a single signal) are impacted by fluorophore leakage, photobleaching, local dye distribution and other minor changes in environmental conditions. This greatly reduces the accuracy and reliability of pH quantification, particularly in the context of intracellular imaging.[58,66–68]

Quantum yields were determined with reference to rhodamine 101, a preferred standard for red emitting fluorophores.[69,70] The neutral species, with a fluorescence lifetime of 3.53 ns, had a desirable quantum yield of 0.35 while the anionic naphtholate possessed a lower quantum yield (Φ = 0.086) and associated lifetime (1.21 ns). Considering absorptivity, the total brightness of the neutral naphthol was calculated to be greater than that of the naphtholate by a factor of 2.3. In addition to the demonstrated capability of SNAFL-C to function as a single molecule ratiometric pH sensor, the distinct lifetimes of the species show excellent applicability in fluorescence lifetime imaging techniques.[71]

3.2.2 Miktoarm polymer conjugate (μ_2). The direct comparison of fluorophore SNAFL-C and labelled polymer μ_2 required a judicious choice of conditions. To isolate the properties of the amphiphilic polymer from its self-assembled structures, an organic solvent system was employed. An ethanolic potassium hydroxide solution with minimal water content was capable of solubilizing both SNAFL-C and its polymeric conjugate, inhibiting self-assembly processes, and pushing the equilibrium to a single fluorescent species (the deprotonated naphtholate). The optical properties of both SNAFL-C and the labelled miktoarm polymer in this medium were evaluated (Table 2). The general absorption and emission profiles of both

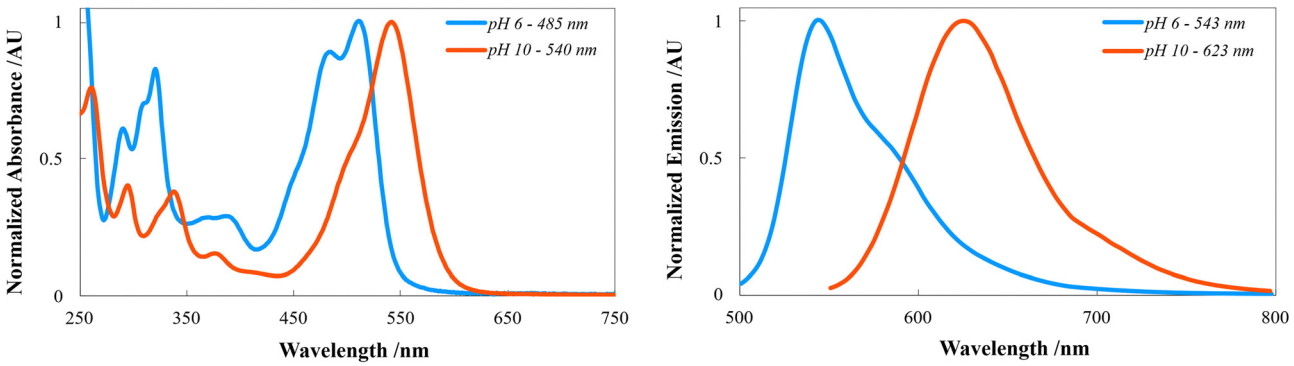

Fig. 1 Normalized absorption and emission spectra of SNAFL-C at pH 6 (naphthol, PBS buffer, λ_{ex} = 485 nm) and pH 10 (naphtholate, carbonate/bicarbonate buffer, λ_{ex} = 540 nm).

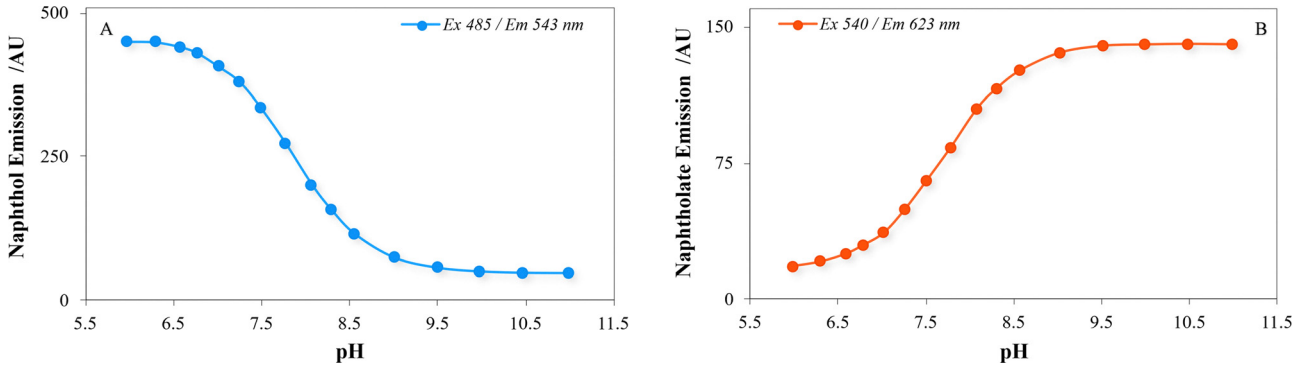

Fig. 2 Ratiometric emission of SNAFL-C with (A) naphthol excited at 485 nm and monitored at 543 nm (B) naphtholate excited at 540 nm and monitored at 623 nm.

Table 2 Optical properties of SNAFL-C (free) and conjugate $\boldsymbol{\mu_2}$ in ethanolic potassium hydroxide

State	λ_{abs}/nm	λ_{em}/nm	Stokes/nm	Φ_f	τ/ns
Free	553	629	76	0.22 ± 0.02	2.65
Conjugated	560	638	78	0.15 ± 0.02	2.08

SNAFL-C and $\boldsymbol{\mu_2}$, seen in Fig. 3, mirrored that of the naphtholate species generated in alkaline aqueous solutions. For SNAFL-C, the change in solvent system from buffer to ethanol resulted in 13 and 6 nm redshifts in absorption and emission, respectively. Fluorescein and its close relatives have been documented to experience hypsochromic shifts with increasing hydrogen bonding capability of the solvent, including in water–alcohol binary mixtures.[72–74] SNAFL-C appeared to match fluorescein and other closely related xanthenes in this respect, undergoing a redshift moving from buffered aqueous solution to ethanol.

While fluorescein and a number of other xanthene dyes are known to experience lowered quantum yields and fluorescence lifetimes in an aqueous medium (due to solvent hydrogen bonding effects), benzoxanthenes have to date only been investigated in buffers.[36,38,46] Transition from an aqueous solution to a polar organic solvent such as ethanol (while keeping the protolytic form constant) is expected to result in changes in solvation of the singlet and triplet excited states, reducing intersystem crossing and leading to longer fluorescence lifetimes and increased quantum yields. This principle evidently remains valid for SNAFL-C, which was observed to experience marked changes to its overall brightness and lifetime of fluorescence. The quantum yield of the fluorophore in this solvent system ($\Phi = 0.22$) was increased by a factor of $\sim$2.6 from that of the naphtholate in alkaline buffer while the fluorescence lifetime extended to 2.7 ns. The fluorescence rate constant ($k_r = \Phi_f/\tau_f$) remained relatively unchanged between the solvents as expected.

A similar rationale may be applied to the behaviour of $\boldsymbol{\mu_2}$ in ethanolic potassium hydroxide, which was shifted a further 7 nm in absorption and 9 nm in emission from the free fluorophore in the same medium. While the overall amphiphilic star polymer was exceptionally soluble in ethanol, it was expected that the polyethylene glycol chains would be fully extended and stretched while those of the less soluble polycaprolactone block would remain relatively coiled and more tightly packed.[75,76] The chromophore, covalently bound to the hydrophobic arm of the polymer, would likely remain partially in this non-polar local environment. The reduced hydrogen bonding from the solvent, altering solvation of the ground and excited states, would be expected to result in the observed bathochromic shifts. The merit of the choice to isolate single

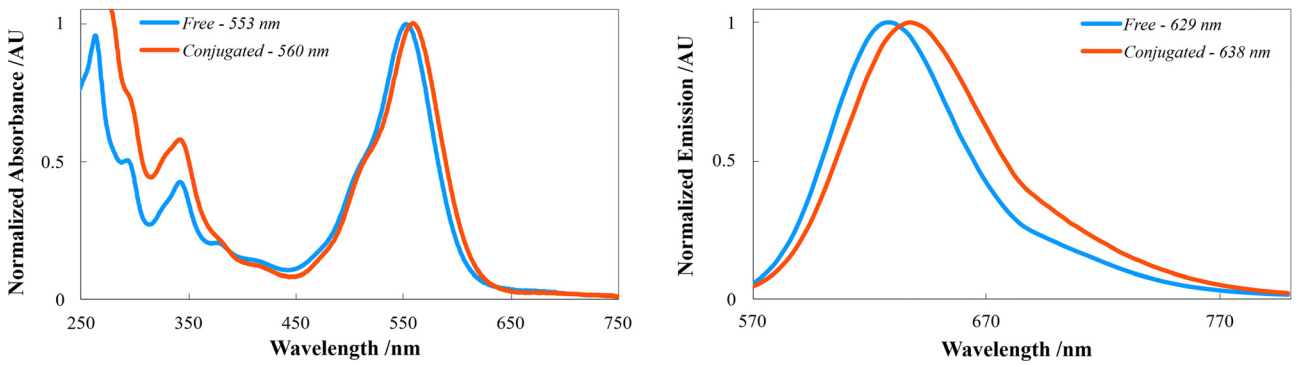

Fig. 3 Normalized absorption and fluorescence emission spectra (λ_{ex} = 560 nm) of SNAFL-C and conjugate $\boldsymbol{\mu_2}$ in ethanolic potassium hydroxide solution.

Table 3 Physical properties of miktoarm star polymers $\boldsymbol{\mu_1}$, $\boldsymbol{\mu_2}$ and their self-assemblies

Polymer			Nanoformulation			
Compound	M_n[a]/g mol^{-1}	$Đ$[b]	Diameter/nm[c]	$Đ$[d]	EE%[e]	LC%
$\boldsymbol{\mu_1}$ (blank)	6600	1.11	30.6 ± 0.4	0.191 ± 0.020	—	—
$\boldsymbol{\mu_1}$ (encapsulating SNAFL-C)	6600	1.11	36.3 ± 0.5	0.227 ± 0.014	60 ± 2	10.8 ± 0.3
$\boldsymbol{\mu_2}$	7400	1.18	32.4 ± 2.0	0.175 ± 0.022	—	—

[a] Determined by MALDI-TOF analysis. [b] Calculated by GPC. [c] Hydrodynamic diameter by DLS. [d] Polydispersity of nanoparticles by DLS. [e] Encapsulation efficiency and loading capacity measured by UV-vis absorbance. Parameters relating to nanoformulations reported as mean ± standard deviation of three separately prepared samples.

isomer SNAFL-C rather than to employ an isomeric mixture for esterification was reflected in the quantum yield of the conjugate. In comparison to the free fluorophore in basic ethanol, conjugate $\boldsymbol{\mu_2}$ exhibited only a modest decrease in quantum yield, thus preserving the overall brightness of the system.

3.3 Nanoparticle self-assembly

Nanoparticles were prepared through aqueous self-assembly using the co-solvent evaporation method: (i) in which SNAFL-C was physically encapsulated in $\boldsymbol{\mu_1}$; and (ii) from $\boldsymbol{\mu_2}$, in which the fluorophore was covalently linked to the polymeric system. Acetone, a low boiling and water miscible solvent, was chosen as the organic phase for its ability to solubilize both $\boldsymbol{\mu_1}$/$\boldsymbol{\mu_2}$, and fluorophore SNAFL-C. Based on the hydrophilic fractions of $\boldsymbol{\mu_1}$ and $\boldsymbol{\mu_2}$, spherical micelles with a core–shell structure were expected.[77] The hydrodynamic diameters of blank and SNAFL loaded $\boldsymbol{\mu_1}$ micelles were measured by dynamic light scattering to be 30.6 ± 0.4 nm and 36.3 ± 0.5 nm, respectively (Table 3). TEM analysis (Fig. S.36) confirmed the presence of spherical nanoparticles of low polydispersity. Assembled $\boldsymbol{\mu_2}$ was seen to largely resemble blank $\boldsymbol{\mu_1}$ nanoparticles, with a hydrodynamic diameter of 32 ± 2 nm. In the nanoparticles physically encapsulating the fluorophore guest, with a SNAFL-C/polymer feed ratio of 20%, we obtained an encapsulation efficiency of 60% and loading capacity of 11%.

Table 4 Optical properties of encapsulated SNAFL-C and assembled $\boldsymbol{\mu_2}$ in pH 10 buffer (naphtholate)

State	λ_{abs}/nm	λ_{em}/nm	Stokes/nm	Φ_f	τ/ns
Encapsulated	541	623	88	0.085 ± 0.008	1.17
Conjugated	550	635	85	0.029 ± 0.003	1.13

3.4 Spectral and photophysical characterization of nanoparticles

The spectral and photophysical properties of the two nanoformulations, SNAFL-C physically encapsulated in nanoparticles of miktoarm $\boldsymbol{\mu_1}$ and self-assembled conjugate $\boldsymbol{\mu_2}$, were investigated (Table 4). The absorption spectrum of each formulation was measured first over the pH range 6–11, as illustrated in Fig. 4. Encapsulated SNAFL-C mirrored the free species to a high degree, with the only variation being a minor decrease in absorptivity at pH 6. This decrease in absorbance eliminated the isosbestic point observed in the corresponding titration of the free fluorophore. While the $\boldsymbol{\mu_2}$ unimer (isolated in basic ethanol) was seen to largely mimic the absorbance and emission characteristics of SNAFL-C, self-assembly of the amphiphile induced significant changes. Absorbance was observed to broaden across the full range of solution pH, with an increase in the full width at half maximum (FWHM) from 66.5 nm for free and encapsulated SNAFL-C to 85.5 nm for assembled $\boldsymbol{\mu_2}$ at pH 10. While the maximum absorbance of the encapsulated species was shifted a mere 1 nm from that of the free species, self-assembled $\boldsymbol{\mu_2}$ exhibited a 10 nm bathochromic shift at pH 10. Identification of self-assembly as the trigger of these features, as supported by the optical properties of the conjugate unimer, suggested meaningful changes in the microenvironment of the $\boldsymbol{\mu_2}$ fluorophore with the formation of nanoparticles.

Analogous to the solvent effects demonstrated for free SNAFL-C, the observed bathochromic shift in absorption may be attributed to partitioning of the fluorophore into the micelle

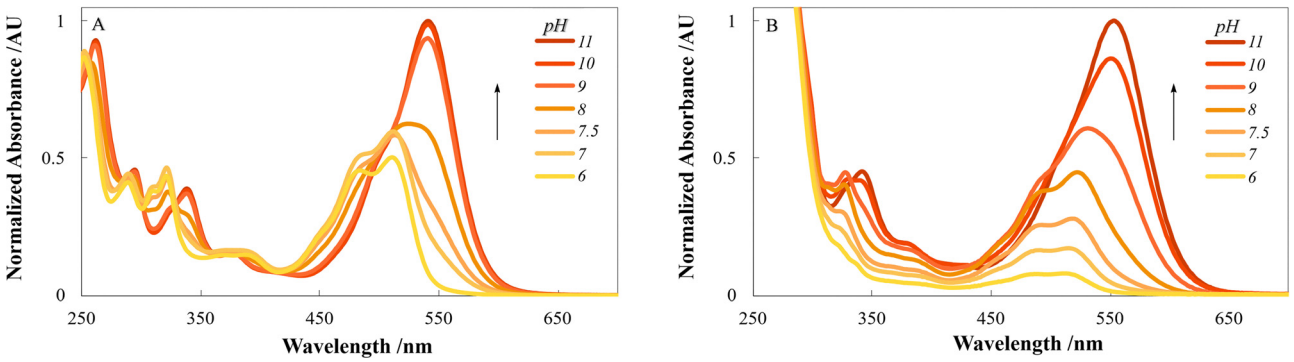

Fig. 4 Absorption spectra of (A) physically encapsulated SNAFL-C and (B) assembled conjugate $\boldsymbol{\mu_2}$ over pH range 6–11.

interior. This transition from an aqueous environment to a 'micellar phase' in which contact with the protic solvent is diminished has been widely reported to lead to redshifts for xanthene dyes.[78–82] In the context of a simplistic core–shell structure with a hydrated polar shell and a non-polar core, only the local environment of the hydrophobic region can be expected to induce these spectral changes. It then follows that the minimal changes in relation to physically encapsulated SNAFL-C are not indicative of meaningful interaction with the polycaprolactone core of the nanostructure. Conversely, the significant bathochromic shifts in absorbance and emission of the assembled conjugate, in which the fluorophore was covalently bound to the polycaprolactone block, suggest partitioning into the hydrophobic core. While the overall bathochromic shifts in the absorbance bands of assembled $\boldsymbol{\mu_2}$ indicated incorporation into the micelle interior, the observed broadening pointed to aggregation effects.

Close packing of aromatic structures (in concentrated solutions, films, and the solid state) almost universally results in aggregation-caused quenching (ACQ), an effect extensively documented for xanthenes.[83–85] The broad category of ACQ, identified originally as 'concentration quenching', encompasses a variety of mechanisms for the reduction of brightness resulting from chromophore contact and interactions. For fluorescein and other xanthenes, quenching is closely tied to the formation of dimers and other supramolecular assemblies, particularly those which may be classified as H-aggregates.[86–90] The entrapment of fluorophores within nanostructures is widely recognized to trigger ACQ effects, diminishing the overall brightness of the system *via* reduced quantum yields.[17,91,92]

The quantum yield of assembled $\boldsymbol{\mu_2}$ was determined to be 0.029 in pH 10 buffer, a reduction of 66% in comparison to free SNAFL-C in the same medium. While the unimer experienced a 32% quantum yield decrease attributed to increased PeT after esterification, the additional 34% reduction may be largely attributed to aggregation effects induced by self-assembly. Similarly, the conjugated naphthol was also seen to undergo a significant decrease in brightness (Table S.2). With the fluorophore end group at a high concentration (5.8% by mass, representing 340 μM in the undiluted formulation) ACQ effects can be expected to be at play. However, SNAFL-C encapsulated nanoparticles did not exhibit the tell-tale signs of ACQ despite a comparatively high formulation concentration of the fluorophore (11% by mass, corresponding to 700 μM in the undiluted formulation). Rather, the absorbance over a wide range of pH values mirrored that of the free fluorophore and the quantum yield of the self-assembly was calculated to be within error of the corresponding value for the free fluorophore for both the naphthol and naphtholate species. These observations indicated a potential lack of spatial confinement (and thus close species contacts) of physically incorporated SNAFL-C, a contrast to the common imagery of encapsulated guests packing neatly into the hydrophobic interior regions of nanostructures.

3.5 Fluorophore localization within nanostructures

To further probe localization with respect to each nanoformulation, fluorescence quenching experiments were carried out. The role of the iodide anion in suppressing xanthene fluorescence *via* dynamic quenching has been well documented.[93–95] This bimolecular reaction competes with the radiative fluorescence process as described by the following equation, in which I_0 represents fluorescence intensity prior to quencher addition and I is the intensity at a given concentration Q of the quencher.

$$\frac{I}{I_0} = 1 + K_{SV}[Q]$$

This phenomenon has in recent years been creatively utilized to ascertain information on the position of xanthene photosensitizers in nanostructures.[78–80,96,97] In the context of core–shell structures the water-soluble iodide ion can in principle only access fluorophores localized in the aqueous corona. Species embedded in a dense hydrophobic core are by extension unlikely to participate in collisions with the quencher. When compared directly to the free compound, Stern Volmer quenching constants (K_{SV}) are expected to decrease when the guest is localized in the core and remain relatively unchanged if dispersed in the shell. The seminaphthofluorescein system provides a unique opportunity to explore the quenching, and by extension localization, of two fluorescent species individually. In order to observe both the SNAFL naphthol and naphtholate simultaneously, all quenching experiments were carried out at pH 7.4, a condition ensuring both species were present in solution. With respect to SNAFL-C the Stern Volmer constants were determined to be 18 (K_{SV}-A) and 3.2 (K_{SV}-B) M^{-1} for the neutral and anionic components, respectively (Table 5). Upon encapsulation of the fluorophore K_{SV}-A underwent a moderate decrease of 18% while K_{SV}-B remained unchanged within error. This was accompanied by spectral data indicating a ~1 nm redshift of the encapsulated naphthol and no observable difference in the naphtholate emission profile (Fig. S.87 and S.88). When the fluorophore was covalently bound (assembled $\boldsymbol{\mu_2}$) K_{SV}-A was decreased by 63% in addition to a 6 nm bathochromic shift. K_{SV}-B experienced a minor increase with no spectral changes associated with the naphtholate being observed.

The combined quenching and spectral evidence suggested marked differences in localization of the fluorescent species within the nanostructures. Generally, the neutral naphthol demonstrated an affinity for the hydrophobic core while the charged and more water soluble naphtholate preferentially remained in the hydrophilic corona region. These observations were consistent with reports of hydrophobicity and reduced charge encouraging the partitioning of xanthenes into non-

Table 5 Stern Volmer quenching constants of free SNAFL-C, encapsulated SNAFL-C, and assembled $\boldsymbol{\mu_2}$ isolated for (A) naphthol (λ_{ex} = 485 nm) and (B) naphtholate (λ_{ex} = 540 nm) species

State	K_{SV}^{A}/M^{-1}	K_{SV}^{B}/M^{-1}
Free	18 ± 1	3.2 ± 0.4
Encapsulated	14.7 ± 0.5	3.1 ± 0.1
Conjugated	6.6 ± 0.2	4.5 ± 0.2

polar core regions of soft nanoparticles.[62,65] The linearity of all Stern Volmer plots with respect to the two nanoformulations (Fig. S.84–S.86) indicated narrow distributions of each species, a direct contrast to the regions of differing slops which emerge when multiple populations of the guest exist in separate microenvironments. With respect to physical encapsulation, the two species were seen to operate independently and partition into the nanocarrier based on their physiochemical properties. The observations of a minor red shift and slightly reduced K_{SV}-A for the naphthol, a moderately hydrophobic species with low charge density, indicated only shallow incorporation into the polycaprolactone core or localization in an intermediate core–shell boundary region. Conversely, the unchanged K_{SV}-B and emission profile supported localization of the naphtholate exclusively in the hydrated shell. For the covalently linked fluorophore, the flexibility of the polycaprolactone chains appeared to allow for organization based on the state of the end group in a similar manner to the encapsulated species. The anionic naphtholate was seen to remain distributed in the corona at neutral pH, avoiding the accumulation of a high charge density in the spatially confined core region. In contrast, the significant bathochromic shift and major reduction of K_{SV} for the naphthol species clearly indicated deep localization in the non-polar core. The emergence of aggregation caused quenching effects in assemblies with covalently linked SNAFL-C ($\boldsymbol{\mu_2}$) was rational considering the observation of a significant portion of the total population of species localizing in the confined hydrophobic core. In the case of encapsulated SNAFL-C, the minimal interaction of either species with the polycaprolactone micelle interior and resulting lack of spatial confinement could be tied to the absence of ACQ, despite the extremely high concentration of the fluorophore in the overall formulation.

While an analysis of quenching and spectral shifts at neutral pH allowed for a simultaneous exploration of the individual localization behaviour of the coexisting species, the behaviour of the covalently linked fluorophore deviated in highly alkaline conditions. In a neutral solution of pH 7.4 the tethered anionic naphtholate was seen to orient in the hydrated corona, matching the emission maximum of the free species and exhibiting no reduction in K_{SV}. However, as the solution pH increased a marked bathochromic shift was observed (totalling 12 nm at pH 10, Fig. S.63). The progressive redshift as the equilibrium was pushed towards complete naphtholate dominance indicated increasing incorporation of the anion in the hydrophobic core. Despite the logical orientation of the highly charged naphtholate end group towards the hydrated shell, covalent attachment of the species to the hydrophobic block appeared to lead to significant interaction of the anion with the nonpolar core at high pH. In these conditions, where the ratio of naphtholate to naphthol species is exceptionally high, total rearrangement of a bulk of the polycaprolactone chains to position these end groups in the polar shell evidently cannot occur, leaving a significant population of the anion in the core microenvironment. This phenomenon was not observed for formulations in which SNAFL-C was physically encapsulated, a case in which mobility of the fluorophore species within the core–shell structure would not be constrained in the same manner as conjugate $\boldsymbol{\mu_2}$.

3.6 Impact of conjugation and assembly – protolytic equilibria

An important nuance of the incorporation of a fluorophore in nanoparticles is the perturbation of protolytic equilibria. For pH sensors such as SNAFL-C, successful application in imaging contexts hinges on the accuracy of relevant protolytic constants. Changes in the microenvironment of a fluorophore in the vicinity of a surfactant, including local polarity differences and hydrogen bonding effects, have been reported to impact equilibrium constants.[78,98,99] The primary pK_a of interest relevant to imaging of these systems relates to the equilibrium between the naphthol and naphtholate species. Determination of this pK_a for SNAFL-C and related ratiometric benzoxanthenes is best carried out by the high sensitivity 'two excitation, two emission' method described by Whitaker *et al.*[38] For each solution of a measured pH, the two species are excited individually and measured at their characteristic wavelengths. The following equation was utilized for pK_a determination.

$$\mathrm{pH} = \mathrm{p}K_a - \log[(R - R_{min}/R_{max} - R)\cdot(F_B/F_A)]$$

Here, R represents ratios of emission intensity from naphthol and naphtholate species, with R_{max} and R_{min} as limiting values and the pK_a of the species as the y intercept. The term F_A/F_B was a ratio of emission intensity in maximum acidic and basic solutions, measured at the wavelength on the denominator of R. Relevant data and fitting can be found in the SI (Fig. S.52–S.66).

The pK_a of SNAFL-C determined by this method, 7.81, was utilized as a reference to evaluate the effects of physical encapsulation and conjugate self-assembly (Table 6). The apparent pK_a of encapsulated SNAFL-C was seen to be 7.77, a minor decrease from that of the free fluorophore. This subtle change, nearly within error, was reflected in the pH dependent intensity profiles for both the encapsulated naphthol and naphtholate species, closely mirroring those of free SNAFL-C (Fig. 5A and Fig. S.54). These observations, coupled with clear indications of differing localization of the fluorescent species in the two formulations, were consistent with literature accounts of the equilibria of xanthenes incorporated into non-ionic micelles. Minor differences in apparent pK_a point towards an equal availability of protons in the vicinity of the fluorophore in comparison to the free species in water. The hydrated polyethylene glycol corona, where encapsulated SNAFL-C was seen to primarily localize, provides such an environment. In addition,

Table 6 Equilibrium constants for free SNAFL-C, encapsulated SNAFL-C, and assembled $\boldsymbol{\mu_2}$

State	pK_a	pK_L
Free	7.81 ± 0.01	4.33 ± 0.01
Encapsulated	7.77 ± 0.02	4.94 ± 0.01
Conjugated	8.04 ± 0.02	5.56 ± 0.03

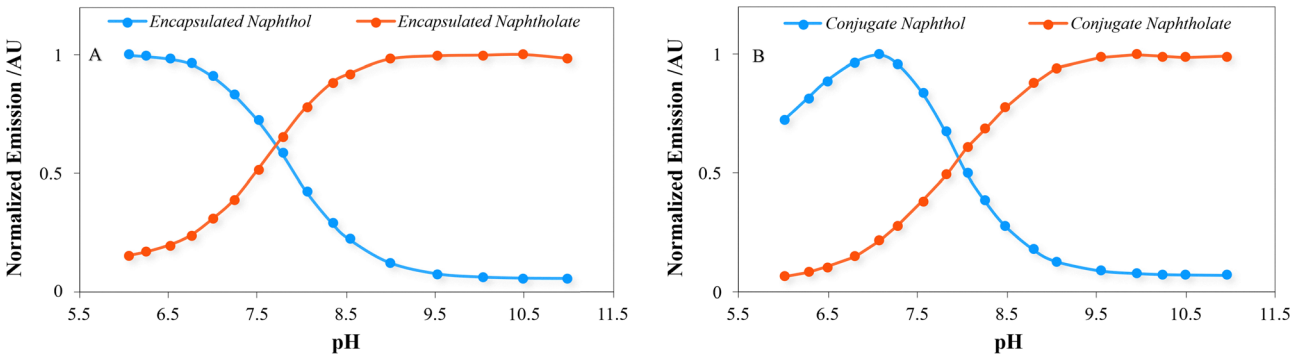

Fig. 5 Visualized equilibrium between (A) encapsulated SNAFL-C naphthol (λ_{ex} = 485 nm, λ_{em} = 543 nm) and naphtholate (λ_{ex} = 540 nm, λ_{em} = 623 nm) in comparison to (B) assembled $\boldsymbol{\mu_2}$ naphthol (λ_{ex} = 485 nm, λ_{em} = 549 nm) and naphtholate (λ_{ex} = 540 nm, λ_{em} = 635 nm).

the absence of aggregation caused quenching effects is likely to contribute to the lack of significant apparent pK_a alteration. Conversely, the pK_a of the self-assembled conjugate, at 8.04, differed more significantly from that of free and physically encapsulated SNAFL-C. While phenolic pK_a values are expected to decrease with incorporation in a region of reduced H^+ availability, as in the case of the conjugated fluorophore which partitioned strongly into the hydrophobic core of the assembly, the opposite was observed here.[78,100] This result may be traced primarily to major differences in the normalized emission profile of the conjugated naphthol, evident in Fig. 5B.

While naphthol emission reached a maximum at pH 6.0 when SNAFL was both free and encapsulated, this extreme occurred at pH 7.0 for assembled $\boldsymbol{\mu_2}$. Moving from pH 11 to pH 7 naphthol fluorescence rose rapidly, in line with the increased apparent pK_a. As seen in Fig. 5B, naphthol emission dropped off steeply between pH 7 and 6. This was accompanied by notably low absorptivity at pH 6 (Fig. S.41). While aggregation effects were known to be at play, these are expected to be relevant over the full range of pH conditions and are not documented to be associated with decreased extinction coefficients. These observations indicated the presence of a secondary equilibrium, forming a weakly absorbing and minimally fluorescent species, occurring below pH 7. While the naphthol–naphtholate equilibrium determined the primary relevant properties of SNAFL-C, a secondary transformation was seen to become significant in highly acidic solutions. This lactonization process, illustrated in Scheme 5, has not previously been

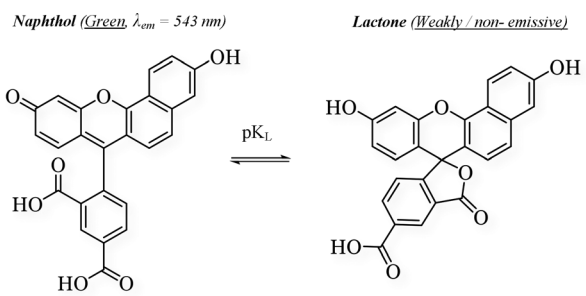

Scheme 5 Equilibrium between SNAFL-C naphthol and ring closed lactone species.

evaluated in detail for SNAFL-C beyond the initial prototropic equilibrium proposed by Whitaker *et al.*[38] The associated equilibrium constant was denoted here as pK_L with calculated values presented in Table 6. For intracellular imaging applications, an environment spanning a wide pH range, a sound understanding of this ring closure equilibrium is essential. This lactone is understood to be generated from the naphthol species, both in highly acidic aqueous solutions and in non-polar organic solvents.[23,101,102] The low absorptivity and weakly emitting nature of this species introduces complexity to its detection. Here, appearance of the lactone was monitored indirectly *via* the decay of naphthol fluorescence. While further transformation of the lactone to the corresponding cationic ring closed compound has been observed for seminaphthofluorescein and simple fluoresceins, this cation was observed primarily at negative pH and can be expected to have a similarly negligible quantum yield.[23,38]

The equilibrium was first investigated for free SNAFL-C in an aqueous medium. Maximum emission of the naphthol species occurred at pH 6, the condition at which concentrations of naphtholate and the non-fluorescent lactone are minimized. Gradual acidification of the solution revealed the anticipated decay of fluorescence corresponding with formation of the ring closed structure. The plateau to minimum fluorescence, seen in Fig. 6A, was observed below pH 2 with a corresponding pK_L of 4.33. Encapsulated SNAFL exhibited similarities to the free species with maximum emission from the naphthol occurring at pH 6. However, a more complete depletion of fluorescence occurred, with nearly no naphthol signal observed below pH 3.5. The pK_L of encapsulated SNAFL-C was calculated to be 4.94, a significant increase from that of the free fluorophore. As partially observed in the titration of the conjugate between pH 6 and 11, the behaviour of assembled $\boldsymbol{\mu_2}$ in the acidic regime diverged from that of the physically encapsulated fluorophore. Rather than reaching a maximum at pH 6.0, emission from the naphthol species continued to increase up to pH 7.0. The corresponding pK_L, 5.56, reflected these marked differences in the lactonization equilibrium. The more significant alterations to pK_L in comparison to pK_a, totalling over a unit with respect to the assembled conjugate, are likely to reflect differences in localization of the lactone. With respect to the

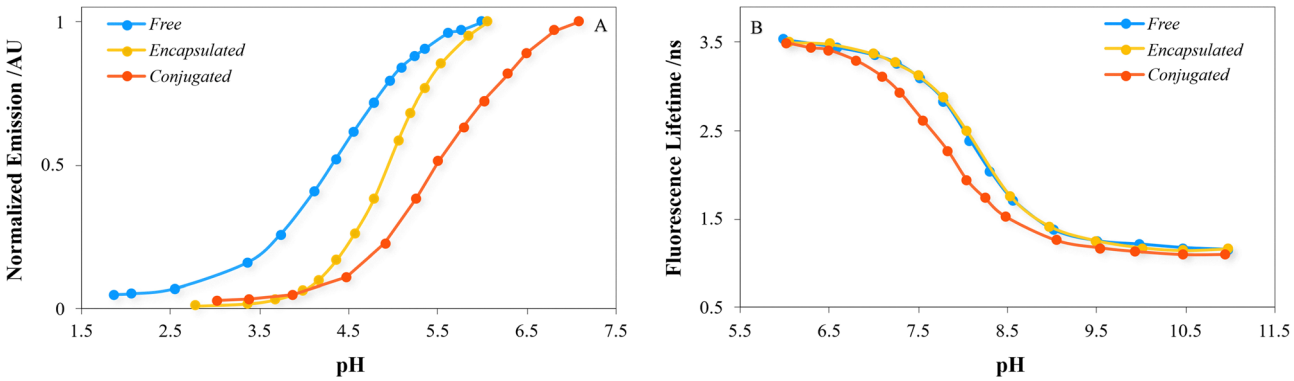

Fig. 6 (A) Decay of naphthol fluorescence in the acidic pH regime demonstrating formation of the SNAFL-C lactone; and (B) fluorescence lifetimes of free SNAFL-C, encapsulated SNAFL-C, and assembled conjugate $\boldsymbol{\mu_2}$.

encapsulated species, where the naphthol and naphtholate were seen to be located primarily in the core/shell boundary and outer shell, the physically incorporated lactone is expected to partition deeper in the polycaprolactone core as a result of its hydrophobicity and reduced charge. The confined core microenvironment, with limited access to protons, distinct polarity differences, and ACQ effects, lends itself to a more significant modulation of equilibrium constants. This effect is logically amplified for formulations of the conjugate, where a population of end group fluorophores were already seen to localize in the core in the 6–11 pH range.

The functionality of free, encapsulated and conjugated SNAFL-C in the context of lifetime-based imaging methodologies was then briefly investigated. While SNAFL-C (like its commercial counterpart SNARF-C) has potential for applicability in fluorescence lifetime imaging, this translation has remained largely unexplored. Time resolved techniques like fluorescence lifetime imaging microscopy (FLIM) are functional both as a stand-alone technique and as a tool to provide an additional layer of information to traditional imaging methods.[103,104] Fig. 6B illustrates the pH dependent fluorescence lifetimes of free and nano-formulated SNAFL. As predicted by the numerous parallels between free and encapsulated SNAFL-C in the standard 6 to 11 pH region, there were no discernible distinctions in their pH dependent lifetime curves. Conversely, the observed differences in the lifetime profile of the assembled conjugate reflected the complexity of protolytic equilibria in the $\boldsymbol{\mu_2}$ system. In the studied pH range the assembled conjugate exhibited lowered lifetimes with respect to both free and encapsulated SNAFL. The curve visually indicated a lowered pK_a, imitating the decay of the conjugated naphtholate in this range. Here, the diminished brightness of the naphthol component in comparison to that of the naphtholate appeared to skew the detected lifetimes to primarily reflect the behaviour of the latter. These results indicated physically incorporated SNAFL could be utilized in the same manner as the free fluorophore for lifetime imaging with no major adjustments while the $\boldsymbol{\mu_2}$ nanoformulation would be expected to require further optimization prior to practical application.

3.7 Biological evaluation

Considering the defined pH response of SNAFL-C and its nanoformulations, we evaluated if these changes could also be observed in a more complex biological environment. Here, the model cells selected for this exploration were human glioblastoma (GBM). Intracellular pH imaging was investigated for free SNAFL-C and diacetate **4**, in addition to two nanoformulations (encapsulated and conjugated). Prior to imaging we assessed cell viability to determine the concentration range which was non-toxic. Under concentrations of 50 μM there was no significant cytotoxicity observed for the any of the four samples (Fig. S.91). In all imaging experiments we utilized low concentrations well within this range (1.5 μM). The two fluorescent species in the prototropic equilibrium of SNAFL were detected separately *via* the use of individual excitation wavelengths and appropriate emission filters. In the specific case of SNAFL-C, the 80 nm separation in emission bands between the two species and 55 nm difference in excitation wavelengths was crucial to the practical imaging of ratiometric emission. While the naphthol was best suited to the GFP filter and represented as green in the subsequent figures, it is relevant to note that naphthol emission was redshifted 28 nm from fluorescein, a fluorophore traditionally associated with green fluorescence.[23,48]

SNAFL-C, introduced as compound **3**, was first examined and seen to exhibit two detectable species. As depicted in Fig. 7B, the neutral and anionic species were visible as green and red fluorescence, respectively. In some cells the green signal was dominant, while red channel emission from the naphtholate species was comparatively weak. Chloroquine (CQ) was then utilized to increase intracellular pH.[105] Cells were initially treated with chloroquine (CQ, 25 μM, 24 h) and subsequently incubated with SNAFL-C for 30 minutes. The red fluorescence signal increased in intensity after this treatment, consistent with an increase in pH in the local environment of the fluorophore. SNAFL-C was then introduced to the cells in its masked form, diacetate **4**. The function of this compound, beyond its unexpected synthetic function in preparation of the conjugate $\boldsymbol{\mu_2}$, was primarily to chaperone the fluorophore into the cell as its neutral (and thus more

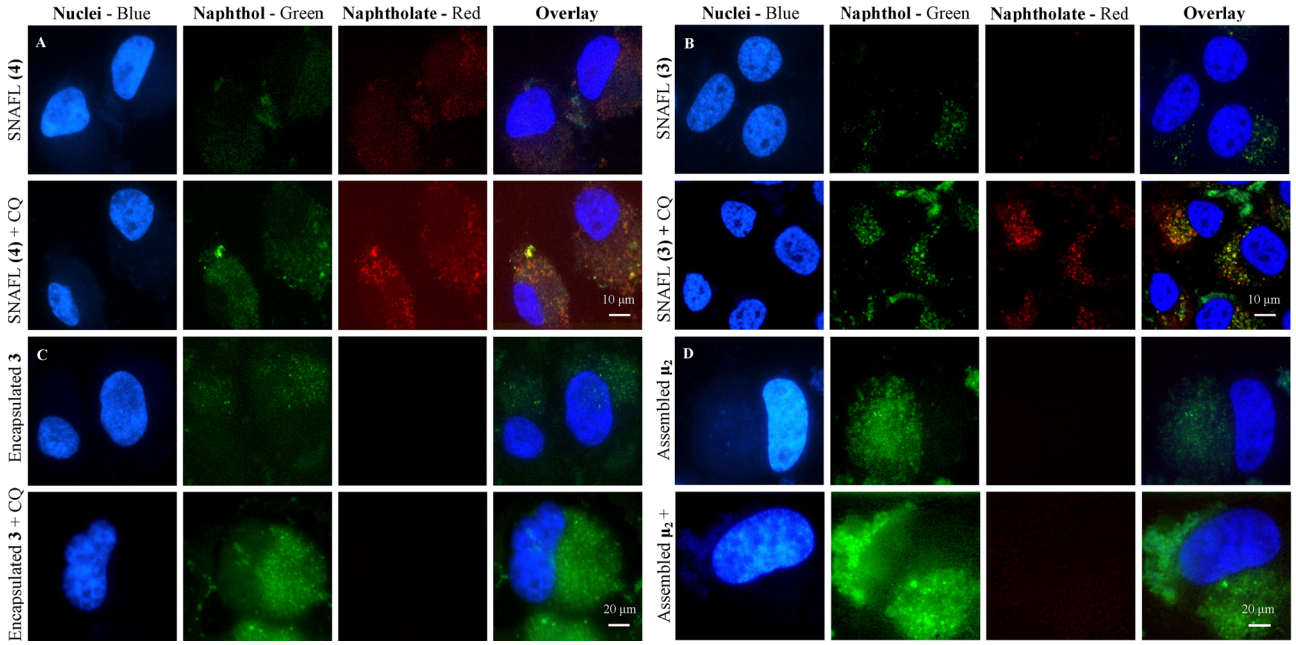

Fig. 7 Detection of (A) free SNAFL-C (compound **3**), (B) SNAFL diacetate (compound **4**), (C) encapsulated SNAFL-C, and (D) assembled conjugate μ_2 in human glioblastoma cells. Cells were treated with chloroquine (CQ, 25 μM) for 24 hours where appropriate. 1.5 μM of the selected fluorophore was added 30 minutes prior to imaging. Species were detected using fluorescent live imaging (GFP green and Cy5 filters); nuclei were labelled with Hoechst 33342 blue.

membrane permeable) non-fluorescent form. Once internalized, the protecting group was expected to be cleaved by intracellular esterases to yield the free fluorophore (SNAFL-C **3**). As seen in direct introduction of SNAFL-C, both red and green signals were observable after 30 minutes of incubation with diacetate **4**, indicating successful cleavage of the acetate moieties. In comparison to incubation with free SNAFL-C, use of the diacetate induced several subtle differences including a minor increase in overall brightness, likely stemming from increased internalization. The relative intensity of the red signal both before and after CQ treatment was moderately higher than those associated with the direct introduction of SNAFL-C. Skewing of this ratio towards the anionic naphtholate indicated a local environment of higher pH experienced by the fluorophore, likely due to minor differences in intracellular localization. The presence of both red and green signals in the initial images as well as the significant increase in the anionic species with CQ treatment pointed towards the local pH experienced by both SNAFL-C **3** and deprotected diacetate **4** as broadly close to neutral.

Cells were then incubated with nanoparticles in which the fluorophore was physically encapsulated or covalently linked. Images derived from incubation with these nanoparticles diverged significantly from those associated with the free fluorophore. For both formulations, before and after pH adjustment, no naphtholate emission was measurable (Fig. 7C and D). The immediately visible dominance of the naphthol species with no detectable signal from the red channel indicated an acidic local environment experienced by the assemblies. For both conjugated and encapsulated SNAFL-C, treatment with chloroquine to increase intracellular pH resulted in increased brightness of the green signal and the continued absence of red emission. Significantly, this further indicated that both nanoparticle formulations were localized in a region of low pH, as informed by investigations of the SNAFL-C lactonization equilibrium. As depicted in Fig. 6A, an increase in solution pH in the acidic regime (under pH 6 for free and encapsulated SNAFL-C and pH 7 for the conjugate) resulted in an increase in emission at the naphthol emission maximum. This was attributed to a shift of the lactone–naphthol equilibrium in which the relative abundance of the weakly fluorescent ring closed species was decreased, with a corresponding increase in the concentration of the green emitting naphthol (Scheme 5). When localized in the acidic lysosomal compartment, both encapsulated and conjugated SNAFL-C would be expected to exhibit increased emission from the green channel with an increase in intracellular pH. The visual indications of an acidic microenvironment experienced by both nanoformulations were consistent with reports showing localization of nanostructures primarily in lysosomes, an organelle with low pH.[13,106–108] Lysosomes, the late endocytic compartment, play a fundamental role in cell function and the regulation of homeostasis, with their malfunction implicated in multiple degenerative disorders.[109,110] Lysosomes have been seen to exhibit heterogeneity between and within cell types, both in terms of their distribution and associated pH.[111] To confirm that the nanoparticles ended up in the lysosomal compartment we utilized LysoTracker™ Red labelling. A significant co-localization of the nanoparticles with LysoTracker Red was observed, indicating that the nanocarriers were delivered to the lysosomal compartments following cellular internalization (Fig. S.90).

4. Conclusions

In this work we employed a holistic approach to the development of a platform to trace the intracellular fate of miktoarm polymer based soft nanoparticles, built on the ratiometric pH sensor SNAFL-C. Our streamlined synthesis of high purity single isomer SNAFL-C contributes to improved accessibility of the fluorophore *via* both vastly diminished costs and acceleration of the isomer separation process. Significantly, the optimized synthetic procedure for ligation of SNAFL-C to the star polymer eliminated the need for additional synthetic tailoring of the fluorophore or polymer end group replacement and did not involve chromatographic purification techniques, as was the case in our preparation of SNAFL-C itself.

Encapsulated SNAFL-C was seen to closely mimic the spectral and photophysical properties of the free fluorophore with no evidence of aggregation caused quenching (ACQ). Nanoparticles of the conjugate also retained several desirable characteristics of SNAFL-C including a high Stokes shift and ratiometric emission despite moderate ACQ effects. This diverging aggregation behaviour between the two formulations was rationalized by a quenching-based assessment which uncovered differing localization of the naphthol and naphtholate species in the core–shell nanostructure. The encapsulated naphthol was seen to be situated at an intermediate core–shell boundary region while the anionic naphtholate remained distributed in the hydrated shell. The clear lack of spatial confinement was consistent with the absence of ACQ despite SNAFL representing an impressive 11% of the total formulation mass, double that of the conjugated formulation. The differences in localization in relation to the conjugated fluorophore (assembled $\boldsymbol{\mu}_2$) were most pronounced at neutral pH. Under these conditions the naphthol was seen to be embedded in the confined hydrophobic core, logically leading to ACQ. The naphtholate localized in the shell, revealing the ability of the structure to reorient polycaprolactone chains with differing end groups according to their physiochemical characteristics. These results emphasized the necessity of evaluating fluorophore incorporated nanocarriers on a highly individual basis with respect to the distinct properties of the guest, including all significant species existing in equilibrium. A change in perspective on ACQ, and methods to investigate it, is of broad importance to the fabrication of fluorescent soft nanoparticles. With respect to the quenching of brightness in nanoformulations, the effect should not be considered directly proportional to concentration, but rather as a more complex issue tied to the individual behaviours of protolytic species and their localization.

SNAFL-C was utilized in live cell fluorescence imaging, demonstrating successful translation to a complex biological environment. The parallel investigation of four formulations (free SNAFL-C **3**, SNAFL-C diacetate **4**, physically encapsulated SNAFL-C, and assembled conjugate $\boldsymbol{\mu}_2$), underpinned by a concrete understanding of the optical properties of the individual systems, enabled clear and direct comparisons. Imaging with respect to both conjugated and physically encapsulated SNAFL-C visually emphasized the differing and highly acidic microenvironment experienced by the internalized nanoparticles in comparison to the free fluorophore. Paired with co-localization experiments, these results indicated delivery of the nanoparticles to the lysosomal compartments of glioblastoma cells. The detailed spectral and photophysical evaluation of SNAFL-C and its nanoformulations, including investigation of the lactonization equilibrium, was a key component in the interpretation of the combined imaging results. Finally, considering these results, we propose that SNAFL-C is not only useful for imaging in glioblastoma cells but in many other cell types, with wide utility in revealing abnormalities in lysosomal and cytoplasmic pH in models of neurological and other disorders.

Author contributions

Conceptualization: L. M., D. M., A. K.; investigations: L. M., N. J.; visualization: L. M.; writing – original draft, review and editing: L. M., D. M., A. K.; supervision: A. K., D. M.; funding acquisition: A. K., D. M.

Conflicts of interest

Authors declare no conflicts of interest.

Data availability

The data supporting this article have been included as part of the SI. Supplementary information: NMR, GPC and other characterization details, together with spectral/photophysical and biological evaluation data, and pricing analysis. See DOI: **https://doi.org/10.1039/d5tb01322d**

Acknowledgements

AK would like to thank the Natural Sciences and Engineering Research Council of Canada (grant number RGPIN-2023-03565), and New Frontiers in Research Fund – Exploration, Canada (grant number NFRFE-2022-00356) for financial assistance. DM thanks the Natural Sciences and Engineering Research Council of Canada (grant number RGPIN 2020-07011) for funding.

References

1 M. J. Mitchell, M. M. Billingsley, R. M. Haley, M. E. Wechsler, N. A. Peppas and R. Langer, *Nat. Rev. Drug Discovery*, 2021, **20**, 101–124.
2 D. Hwang, J. D. Ramsey and A. V. Kabanov, *Adv. Drug Delivery Rev.*, 2020, **156**, 80–118.
3 B. Ghosh and S. Biswas, *J. Controlled Release*, 2021, **332**, 127–147.
4 H. Cabral, K. Miyata, K. Osada and K. Kataoka, *Chem. Rev.*, 2018, **118**, 6844–6892.

5 A. Gagliardi, E. Giuliano, E. Venkateswararao, M. Fresta, S. Bulotta, V. Awasthi and D. Cosco, *Front. Pharmacol.*, 2021, **12**, 601626.
6 Y. Barenholz, *J. Controlled Release*, 2012, **160**, 117–134.
7 D. Peer, J. M. Karp, S. Hong, O. C. Farokhzad, R. Margalit and R. Langer, *Nat. Nanotechnol.*, 2007, **2**, 751–760.
8 A. K. Pearce, A. B. Anane-Adjei, R. J. Cavanagh, P. F. Monteiro, T. M. Bennett, V. Taresco, P. A. Clarke, A. A. Ritchie, M. R. Alexander, A. M. Grabowska and C. Alexander, *Adv. Healthcare Mater.*, 2020, **9**, 2000892.
9 A. Kakkar, G. Traverso, O. C. Farokhzad, R. Weissleder and R. Langer, *Nat. Rev. Chem.*, 2017, **1**, 0063.
10 A. B. Cook and S. Perrier, *Adv. Funct. Mater.*, 2020, **30**, 1901001.
11 M. Liu, J. R. Blankenship, A. E. Levi, Q. Fu, Z. M. Hudson and C. M. Bates, *Chem. Mater.*, 2022, **34**, 6188–6209.
12 S. Behzadi, V. Serpooshan, W. Tao, M. A. Hamaly, M. Y. Alkawareek, E. C. Dreaden, D. Brown, A. M. Alkilany, O. C. Farokhzad and M. Mahmoudi, *Chem. Soc. Rev.*, 2017, **46**, 4218–4244.
13 R. Savić, L. Luo, A. Eisenberg and D. Maysinger, *Science*, 2003, **300**, 615–618.
14 N. P. Truong, M. R. Whittaker, C. W. Mak and T. P. Davis, *Expert Opin. Drug Delivery*, 2015, **12**, 129–142.
15 Q. Yu, M. G. Roberts, L. Houdaihed, Y. Liu, K. Ho, G. Walker, C. Allen, R. M. Reilly, I. Manners and M. A. Winnik, *Nanoscale*, 2021, **13**, 280–291.
16 S. Bou, A. S. Klymchenko and M. Collot, *Mater. Adv.*, 2021, **2**, 3213–3233.
17 A. Reisch and A. S. Klymchenko, *Small*, 2016, **12**, 1968–1992.
18 M. P. Robin and R. K. O'Reilly, *Polym. Int.*, 2015, **64**, 174–182.
19 S. Kunjachan, J. Ehling, G. Storm, F. Kiessling and T. Lammers, *Chem. Rev.*, 2015, **115**, 10907–10937.
20 T. Etrych, H. Lucas, O. Janoušková, P. Chytil, T. Mueller and K. Mäder, *J. Controlled Release*, 2016, **226**, 168–181.
21 J. S. D. Mieog, F. B. Achterberg, A. Zlitni, M. Hutteman, J. Burggraaf, R.-J. Swijnenburg, S. Gioux and A. L. Vahrmeijer, *Nat. Rev. Clin. Oncol.*, 2022, **19**, 9–22.
22 M. F. Marmor and J. G. Ravin, *Arch. Ophthalmol.*, 2011, **129**, 943–948.
23 R. Sjöback, J. Nygren and M. Kubista, *Spectrochim. Acta, Part A*, 1995, **51**, L7–L21.
24 J. Yan, Z. Ye, H. Luo, M. Chen, Y. Zhou, W. Tan, Y. Xiao, Y. Zhang and M. Lang, *Polym. Chem.*, 2011, **2**, 1331–1340.
25 F. Thielbeer, S. V. Chankeshwara and M. Bradley, *Biomacromolecules*, 2011, **12**, 4386–4391.
26 S. Kumar Panigrahi and A. Kumar Mishra, *J. Photochem. Photobiol., C*, 2019, **41**, 100318.
27 T.-B. Ren, W. Xu, W. Zhang, X.-X. Zhang, Z.-Y. Wang, Z. Xiang, L. Yuan and X.-B. Zhang, *J. Am. Chem. Soc.*, 2018, **140**, 7716–7722.
28 L. D. Lavis and R. T. Raines, *ACS Chem. Biol.*, 2014, **9**, 855–866.
29 D. Seah, Z. Cheng and M. Vendrell, *ACS Nano*, 2023, **17**, 19478–19490.
30 M. Dai, Y. J. Yang, S. Sarkar and K. H. Ahn, *Chem. Soc. Rev.*, 2023, **52**, 6344–6358.
31 H. Chen, B. Dong, Y. Tang and W. Lin, *Acc. Chem. Res.*, 2017, **50**, 1410–1422.
32 H. Lu, J. Mack, Y. Yang and Z. Shen, *Chem. Soc. Rev.*, 2014, **43**, 4778–4823.
33 R. Weissleder, *Nat. Biotechnol.*, 2001, **19**, 316–317.
34 R. S. DaCosta, H. Andersson and B. C. Wilson, *Photochem. Photobiol.*, 2003, **78**, 384–392.
35 L. G. Lee, G. M. Berry and C.-H. Chen, *Cytometry*, 1989, **10**, 151–164.
36 E. Azuma, N. Nakamura, K. Kuramochi, T. Sasamori, N. Tokitoh, I. Sagami and K. Tsubaki, *J. Org. Chem.*, 2012, **77**, 3492–3500.
37 Z. Khan and N. Sekar, *Dyes Pigm.*, 2023, **208**, 110735.
38 J. E. Whitaker, R. P. Haugland and F. G. Prendergast, *Anal. Biochem.*, 1991, **194**, 330–344.
39 O. Seksek, N. Henry-Toulmé, F. Sureau and J. Bolard, *Anal. Biochem.*, 1991, **193**, 49–54.
40 M. Yassine, J.-M. Salmon, J. Vigo and P. Viallet, *J. Photochem. Photobiol., B*, 1997, **37**, 18–25.
41 M. Beija, C. A. M. Afonso and J. M. G. Martinho, *Chem. Soc. Rev.*, 2009, **38**, 2410–2433.
42 J. E. Whitaker, R. P. Haugland, D. Ryan, P. C. Hewitt, R. P. Haugland and F. G. Prendergast, *Anal. Biochem.*, 1992, **207**, 267–279.
43 M. Li, O. Rouaud and D. Poncelet, *Int. J. Pharm.*, 2008, **363**, 26–39.
44 K. Kalyanasundaram and J. K. Thomas, *J. Am. Chem. Soc.*, 1977, **99**, 2039–2044.
45 Y. Ueno, G.-S. Jiao and K. Burgess, *Synthesis*, 2004, 2591–2593.
46 P. Hammershøj, E. Thyrhaug, P. Harris, P. K. Ek, T. L. Andresen and M. H. Clausen, *Tetrahedron Lett.*, 2017, **58**, 1611–1615.
47 M. Sibrian-Vazquez, J. O. Escobedo, M. Lowry, F. R. Fronczek and R. M. Strongin, *J. Am. Chem. Soc.*, 2012, **134**, 10502–10508.
48 X.-F. Zhang, J. Zhang and L. Liu, *J. Fluoresc.*, 2014, **24**, 819–826.
49 T. Ueno, Y. Urano, K.-I. Setsukinai, H. Takakusa, H. Kojima, K. Kikuchi, K. Ohkubo, S. Fukuzumi and T. Nagano, *J. Am. Chem. Soc.*, 2004, **126**, 14079–14085.
50 T. Mineno, T. Ueno, Y. Urano, H. Kojima and T. Nagano, *Org. Lett.*, 2006, **8**, 5963–5966.
51 F. M. Rossi and J. P. Y. Kao, *Bioconjugate Chem.*, 1997, **8**, 495–497.
52 A. Brunet, T. Aslam and M. Bradley, *Bioorg. Med. Chem. Lett.*, 2014, **24**, 3186–3188.
53 M. Adamczyk, C. M. Chan, J. R. Fino and P. G. Mattingly, *J. Org. Chem.*, 2000, **65**, 596–601.
54 M. V. Kvach, D. A. Tsybulsky, A. V. Ustinov, I. A. Stepanova, S. L. Bondarev, S. V. Gontarev, V. A. Korshun and V. V. Shmanai, *Bioconjugate Chem.*, 2007, **18**, 1691–1696.
55 P. Hammershøj, E. K. P. Kumar, P. Harris, T. L. Andresen and M. H. Clausen, *Eur. J. Org. Chem.*, 2015, 7301–7309.

56 J. A. Thomas, R. N. Buchsbaum, A. Zimniak and E. Racker, *Biochemistry*, 1979, **18**, 2210–2218.
57 B. Rotman and B. W. Papermaster, *Proc. Natl. Acad. Sci. U. S. A.*, 1966, **55**, 134–141.
58 J. Han and K. Burgess, *Chem. Rev.*, 2010, **110**, 2709–2728.
59 T. J. Rink, R. Y. Tsien and T. Pozzan, *J. Cell Biol.*, 1982, **95**, 189–196.
60 O. Altintas, A. P. Vogt, C. Barner-Kowollik and U. Tunca, *Polym. Chem.*, 2012, **3**, 34–45.
61 A. Hanisch, H. Schmalz and A. H. E. Müller, *Macromolecules*, 2012, **45**, 8300–8309.
62 B. Neises and W. Steglich, *Angew. Chem., Int. Ed. Engl.*, 1978, **17**, 522–524.
63 X. Huang, J. Song, B. C. Yung, X. Huang, Y. Xiong and X. Chen, *Chem. Soc. Rev.*, 2018, **47**, 2873–2920.
64 R. Gui and H. Jin, *J. Photochem. Photobiol., C*, 2024, **58**, 100650.
65 D. Wencel, T. Abel and C. McDonagh, *Anal. Chem.*, 2014, **86**, 15–29.
66 M. J. Boyer and D. W. Hedley, in *Methods in Cell Biology*, ed. Z. Darzynkiewicz, J. Paul Robinson and H. A. Crissman, Academic Press, 1994, vol. 41, pp. 135–148.
67 R. Y. Tsien, in *Methods in Cell Biology*, ed. D. L. Taylor and Y.-L. Wang, Academic Press, 1989, vol. 30, pp. 127–156.
68 R. B. Silver, in *Methods in Cell Biology*, ed. G. Sluder and D. E. Wolf, Academic Press, 1998, vol. 56, pp. 237–251.
69 A. M. Brouwer, *Pure Appl. Chem.*, 2011, **83**, 2213–2228.
70 A. Alessi, M. Salvalaggio and G. Ruzzon, *J. Lumin.*, 2013, **134**, 385–389.
71 H. Szmacinski and J. R. Lakowicz, *Anal. Chem.*, 1993, **65**, 1668–1674.
72 M. M. Martin, *Chem. Phys. Lett.*, 1975, **35**, 105–111.
73 F. Naderi and A. Farajtabar, *J. Mol. Liq.*, 2016, **221**, 102–107.
74 G. R. Fleming, A. W. E. Knight, J. M. Morris, R. J. S. Morrison and G. W. Robinson, *J. Am. Chem. Soc.*, 1977, **99**, 4306–4311.
75 R. Wang and Z.-G. Wang, *Macromolecules*, 2014, **47**, 4094–4102.
76 N.-K. Lee, A. Johner and T. A. Vilgis, *Macromolecules*, 2002, **35**, 6043–6054.
77 Y. Mai and A. Eisenberg, *Chem. Soc. Rev.*, 2012, **41**, 5969–5985.
78 C. F. de Freitas, N. L. da Rocha, I. S. Pereverzieff, V. R. Batistela, L. C. Malacarne, N. Hioka and W. Caetano, *J. Mol. Liq.*, 2021, **322**, 114904.
79 D. S. Pellosi, B. M. Estevão, J. Semensato, D. Severino, M. S. Baptista, M. J. Politi, N. Hioka and W. Caetano, *J. Photochem. Photobiol., A*, 2012, **247**, 8–15.
80 C. F. de Freitas, D. S. Pellosi, B. M. Estevão, I. R. Calori, T. M. Tsubone, M. J. Politi, W. Caetano and N. Hioka, *Photochem. Photobiol.*, 2016, **92**, 790–799.
81 B. B. Bhowmik and P. Ganguly, *Spectrochim. Acta, Part A*, 2005, **62**, 808–813.
82 D. S. Pellosi, B. M. Estevão, C. F. Freitas, T. M. Tsubone, W. Caetano and N. Hioka, *Dyes Pigm.*, 2013, **99**, 705–712.
83 O. Valdes-Aguilera and D. C. Neckers, *Acc. Chem. Res.*, 1989, **22**, 171–177.
84 R. F. Chen and J. R. Knutson, *Anal. Biochem.*, 1988, **172**, 61–77.
85 J. B. Birks, *Photophysics of Aromatic Molecules*, Wiley-Interscience, 1970.
86 I. L. Arbeloa, *J. Chem. Soc., Faraday Trans. 2*, 1981, **77**, 1735–1742.
87 I. López Arbeloa, *J. Photochem.*, 1982, **18**, 161–168.
88 M. Van der Auweraer, B. Verschuere and F. C. De Schryver, *Langmuir*, 1988, **4**, 583–588.
89 K. K. Rohatgi and G. S. Singhal, *J. Phys. Chem.*, 1966, **70**, 1695–1701.
90 B. Heyne, *Photochem. Photobiol. Sci.*, 2016, **15**, 1103–1114.
91 G. Sun, M. Y. Berezin, J. Fan, H. Lee, J. Ma, K. Zhang, K. L. Wooley and S. Achilefu, *Nanoscale*, 2010, **2**, 548–558.
92 A. H. Ashoka, I. O. Aparin, A. Reisch and A. S. Klymchenko, *Chem. Soc. Rev.*, 2023, **52**, 4525–4548.
93 J. Q. Umberger and V. K. LaMer, *J. Am. Chem. Soc.*, 1945, **67**, 1099–1109.
94 W. J. Svirbely and N. E. Sharpless, *J. Am. Chem. Soc.*, 1954, **76**, 1404–1409.
95 A. Chmyrov, T. Sandén and J. Widengren, *J. Phys. Chem. B*, 2010, **114**, 11282–11291.
96 V. Kabanov, D. J. Press, R. P. S. Huynh, G. K. H. Shimizu and B. Heyne, *Chem. Commun.*, 2018, **54**, 6320–6323.
97 I. R. Calori, D. S. Pellosi, D. Vanzin, G. B. Cesar, P. C. S. Pereira, M. J. Politi, N. Hioka and W. Caetano, *J. Braz. Chem. Soc.*, 2016, **27**, 1938–1948.
98 C. F. de Freitas, B. M. Estevão, D. S. Pellosi, I. S. Scarminio, W. Caetano, N. Hioka and V. R. Batistela, *J. Mol. Liq.*, 2021, **327**, 114794.
99 A. Song, J. Zhang, M. Zhang, T. Shen and J. A. Tang, *Colloids Surf., A*, 2000, **167**, 253–262.
100 C. F. de Freitas, D. Vanzin, T. L. Braga, D. S. Pellosi, V. R. Batistela, W. Caetano and N. Hioka, *J. Mol. Liq.*, 2020, **313**, 113320.
101 V. R. Batistela, J. da Costa Cedran, H. P. Moisés de Oliveira, I. S. Scarminio, L. T. Ueno, A. Eduardo da Hora Machado and N. Hioka, *Dyes Pigm.*, 2010, **86**, 15–24.
102 N. Klonis and W. H. Sawyer, *J. Fluoresc.*, 1996, **6**, 147–157.
103 W. Becker, *J. Microsc.*, 2012, **247**, 119–136.
104 W. Becker, A. Bergmann, M. A. Hink, K. König, K. Benndorf and C. Biskup, *Microsc. Res. Tech.*, 2004, **63**, 58–66.
105 P. Pellegrini, A. Strambi, C. Zipoli, M. Hägg-Olofsson, M. Buoncervello, S. Linder and A. De Milito, *Autophagy*, 2014, **10**, 562–571.
106 S. T. G. Street, Y. He, X.-H. Jin, L. Hodgson, P. Verkade and I. Manners, *Chem. Sci.*, 2020, **11**, 8394–8408.
107 K.-I. Joo, L. Xiao, S. Liu, Y. Liu, C.-L. Lee, P. S. Conti, M. K. Wong, Z. Li and P. Wang, *Biomaterials*, 2013, **34**, 3098–3109.
108 P. Srivastava, I. Tavernaro, C. Genger, P. Welker, O. Hübner and U. Resch-Genger, *Anal. Chem.*, 2022, **94**, 9656–9664.
109 A. Raj and U. Bandyopadhyay, *Front. Neurosci.*, 2024, **17**, 1331211.
110 M. Cao, X. Luo, K. Wu and X. He, *Signal Transduction Targeted Ther.*, 2021, **6**, 379.
111 D. Chen and M. G. Gutierrez, *J. Cell Biol.*, 2025, **224**, e202412011.

